Journal of Theoretical Biology 618 (2026) 112311

Contents lists available at ScienceDirect

Journal of Theoretical Biology

journal homepage: www.elsevier.com/locate/jtbi

Rapid cell turnover to model adipocyte size distribution

Louis Fostier [a,b], Aloïs Dauger [c,d], Romain Yvinec [a,b], Magali Ribot [e,f], Chloe Audebert [b,d,g,1,*], Hedi Soula [c,1]

[a] PRC, INRAE, CNRS, Université de Tours, 37380, Nouzilly, France
[b] Université Paris-Saclay, Inria, Centre Inria de Saclay, 91120, Palaiseau, France
[c] Sorbonne Université, Inserm, Nutrition and obesities: systemic approaches, Nutriomics, F-75013, Paris, France
[d] Sorbonne Université, Université Paris Cité, CNRS, Laboratoire Jacques-Louis Lions, LJLL, F-75005, Paris, France
[e] Institut Denis Poisson, Université d'Orléans, CNRS, Université de Tours, 45067, Orléans, France
[f] Université Paris-Saclay,MaIAGE, INRAE, 78350, Jouy-en-Josas, France
[g] Sorbonne Université, CNRS, Laboratoire de Biologie Computationnelle, Quantitative et Synthétique, CQSB, F-75005, Paris, France

ARTICLE INFO

Keywords:
Partial differential equation modeling
Adipocyte size distribution
White adipocyte tissue
Parameter estimation
Stationary solution

ABSTRACT

White adipose tissue, composed of adipocyte cells, primarily stores energy as lipid droplets. The size of adipocytes varies significantly within the tissue according to the amount of stored lipids. A striking observation is that the adipocyte size distribution is bimodal, and thus, this tissue is lacking a characteristic size.

We propose a novel dynamical model, based on a partial differential equation, to represent the adipocyte size distribution. The model assumes continuous adipocyte growth, with a velocity dependent on cell radius and extracellular lipid availability, together with constant rates of cell recruitment and death.

We prove the existence and local stability of a unique stationary solution for a broad range of growth velocity functions. Choosing a parcimonious formulation, we show that only three parameters are enough to describe adipocyte size distributions measurements in rats. These parameters are robustly estimated through approximate Bayesian computation, and the model demonstrates excellent agreement with experimental data. This mechanistic, three-parameter framework offers a new and interpretable approach to characterizing adipocyte size distributions.

1. Introduction

The global public health challenge posed by obesity has drawn significant interest from the scientific community. Defined as an excessive accumulation of white adipose tissue, obesity is associated with an increased risk of comorbidities such as type 2 diabetes, cardiovascular diseases and certain cancers Lim and Boster (2025). These obesity-related diseases are the consequences of white adipose tissue dysfunctions. A chronic energy imbalance results in lipid accretion in cells dedicated to storage, i.e. the adipocytes. This accumulation is enabled by two mechanisms, which are the increase of adipocyte number (hyperplasia) and the increase of adipocyte size (hypertrophy). In fact, adipocytes exhibit singular size properties with radii ranging from 7 μm to 150 μm and displaying a bimodal size distribution with a peak around $10-12$ μm and a second one around $50-60$ μm McLaughlin et al. (2007).

An abnormal size of those cells may be the onset of a complete tissue impairment as it correlates with drastic physiological changes. First, at the cell scale, lipolysis, lipogenesis activity, adrenoceptor expression, insulin sensitivity and senescence are altered Hansen et al. (1974), Lafontan and Berlan (1995), McLaughlin et al. (2007), Wan et al. (2024). Then, at the tissue scale, through permanent crosstalk and interactions with the stroma-vascular fraction, macrophages infiltration, reduced angiogenesis, hypoxia and fibrosis take place Trayhurn (2013), Turner et al. (2022). Finally, alterations are observed at a systemic scale, such as low-grade inflammation, glucose metabolism impairment, altered adipokine secretion and liver steatosis Santoro et al. (2010), McLaughlin et al. (2007), Le Lay et al. (2001), Liu et al. (2010), Skurk et al. (2007). The size and number of adipocytes are key parameters in obesity. Whether they are drivers leading to the pathological state or indicators of it is not yet clear. However, it is widely accepted that they play a pivotal role in the emergence and persistence of obesity.

Several mathematical models have been proposed to better understand adipocyte size dynamics. In Jo et al. (2009, 2010, 2012), authors have proposed models based on partial differential equations to represent adipocyte size distributions in rats under various dietary conditions. They assumed cell turnover and a size-dependent growth rate.

* Corresponding author.
E-mail address: chloe.audebert@sorbonne-universite.fr (C. Audebert).
[1] These authors contributed equally to this work.

https://doi.org/10.1016/j.jtbi.2025.112311
Received 4 June 2025; Received in revised form 8 September 2025; Accepted 30 October 2025
Available online 10 November 2025

In these models, the parameters are difficult to relate to physiological processes. Then, the model in MacKellar et al. (2010) is based on three compartments: small, medium and large adipocytes. The cell size evolution depends on lipid fluxes that are related to protein concentration controlling lipotoxicity – a cellular dysfunction due to lipid accumulation in non-adipose tissue. These models provide studies of adipose tissue growth dynamics and its bimodality through cell hyperplasia and/or hypertrophy. These previous works do not study stationary solutions and rely on large numbers of general parameters. More recently, authors in Cabeza De Baca et al. (2024) have proposed a statistical approach to extract characteristics of cell size distributions for several participants before and after caloric restriction.

In addition, we have previously proposed mechanistic models based on lipid fluxes Soula et al. (2013, 2015), Giacobbi et al. (2024), Meyer et al. (2024), Dauger et al. (2025). These models share common assumptions: a) there is only one adipocyte population type, b) cell size is determined by lipid fluxes, c) the lipid inflow and outflow are proportional to the surface area of the cell, d) the number of cells is constant: apoptosis and recruitment of cells are neglected. These previous models strongly rely on a slow turnover of adipocytes (in humans 10 % of fat cells are renewed annually Spalding et al. (2008)). However, it has been reported that 0.6 % to 1.5 % adipocytes are renewed each day for lean mice ad libitum Rigamonti et al. (2011), Neese et al. (2002), Kim et al. (2014). It requires reconsidering the hypothesis of slow turnover of adipocyte cells in rats (since the measurements considered previously and in this paper are measured in rats).

In this work, we propose a new mathematical model, based on a partial differential equation, that aims at modeling adipocyte size distributions taking into account cell turnover (cell "death" and "recruitment"). New adipocytes enter the population at a constant recruitment rate with a common minimal radius. Cell size over time is related to lipid uptake, assuming outflow of lipids can be neglected. Based on previous mechanical considerations, the magnitude of the uptake depends on the amount of extracellular lipids and on the radius of the cell. The growth velocity is low for small cells due to size-dependent lipid influx, increases to a maximum at an intermediate size, then declines toward zero as radius further increases to reflect tissue constraints. Therefore, cells will accumulate at sizes where the growth rate is low. Assuming a death term with constant rate prevents cells from accumulating at sizes larger than the physiological limit. All these properties allow us to obtain bimodal cell size distributions. The modeling assumptions and equations are described in Section 2.1 and the stationary solution is introduced in Section 2.2. We show that this model admits a unique stationary solution, locally asymptotically stable in Section 3.1. Numerical simulation is performed to explore the model output sensitivity to parameters in Section 3.2 and, then, the model parameters are estimated with adipocyte size distributions measured in rats in Section 3.3. We show that the model is in good agreement with the measurements, with only 3 parameters to estimate. Finally, we conclude this paper with a discussion in Section 4.

2. Model and methods

2.1. Model for adipocyte size distribution

We present in this paper a new model of dynamics of adipocyte size. Adipocytes are cells that do not divide and adipogenesis is driven by pre-adipocyte differentiation Ghaben and Scherer (2019). So, we assume that new adipocytes enter the population at a constant recruitment rate ρ (cell.time^{-1}) with a radius of $r_{\min}$ (μm). This first point is taken into account in the model through a boundary condition at $r = r_{\min}$ (Eq. (2)). We also assume that the cells undergo apoptosis at rate σ (time^{-1}), independent of age and size. This leads to the right hand side of Eq. (1). Moreover, cell incorporates lipids (and thus grows in size) at a speed that depends on its radius r and on the amount of extracellular lipids L (nmol). We assume that the growth speed has a separable form, defined as

$$V(r, L) = f(L)g(r),$$

with f an increasing function of the extracellular lipids L and g a positive continuous function of radius r. The separable form of function V means that extracellular lipids availability and cell size influence lipid uptake independently and in a multiplicative manner. From an analytical point of view, Theorem 3 gives more precise assumptions on functions f and g to prove existence, uniqueness and stability of the stationary solution. At a modeling level, we choose functions f and g as in Eq. (11) to perform parameter estimation.

We obtain therefore a flow equation, that describes the evolution of the cell density $u(t, r)$ at time $t \in \mathbb{R}^+$ with radius $r \in (r_{\min}; +\infty[$, i.e.

$$\frac{\partial}{\partial t}u(t, r) + \frac{\partial}{\partial r}(V(r, L(t))u(t, r)) = -\sigma u(t, r) \tag{1}$$

with boundary condition on $r = r_{\min}$,

$$V(r_{\min}, L(t))u(t, r_{\min}) = \rho. \tag{2}$$

The extracellular (available) lipid quantity L depends on time t: it increases whenever cells die and decreases when cells grow. The decrease depends on the amount of variation of the lipid content of a cell, denoted by $l(r)$, a function of cell radius r. The assumption that lipids are redistributed and never consumed by the body leads to a conservation equation of total lipid amount. We also assume in this paper that the total lipid amount variations can be neglected. Therefore, the content of lipids inside all cells (also called intracellular lipid amount in the following) $L_{\text{int}}(t)$ at time t is given by the expression

$$L_{\text{int}}(t) := \int_{r_{\min}}^{\infty} l(s)u(t, s)\mathrm{d}s, \tag{3}$$

and we express that the total amount of lipids, L_0 (nmol), is constant at all times t by the equation

$$L(t) + L_{\text{int}}(t) = L_0 \text{ for all } t \geq 0. \tag{4}$$

Eqs. (1), (2) and (4) with initial distribution $u(0, r) = u_0(r)$ for all $r > r_{\min}$ define a time-dependent size density function. Using fixed point argument on the function $t \mapsto L(t)$, we show that global existence, uniqueness and non-negativity of solution $u \in \mathrm{L}^1\big((r_{\min}, +\infty), (1 + l(x))\mathrm{d}x\big)$ holds under fairly general assumption. Here, for any measurable weight function ω, $\mathrm{L}^1((r_{\min}, +\infty), \omega(x)\mathrm{d}x)$ denotes the space of all measurable functions f such that $f\omega \in \mathrm{L}^1((r_{\min}, +\infty))$, see e.g. Laurençot (2001), Collet and Goudon (2000), Calvo et al. (2021).

We now give some explicit forms for functions l, f and g. Assuming spherical shape for the adipocytes, we can link l and r as

$$V_l\, l(r) = \frac{4\pi}{3}r^3 - \frac{4\pi}{3}r_{\min}^3, \tag{5}$$

where V_l (μm^3.nmol^{-1}) is a conversion constant Soula et al. (2013) and $r_{\min}$ is the radius of an empty cell.

An adipocyte captures lipids at a rate proportional to its surface area and, as cells cannot grow indefinitely, we assume a decreasing growth speed for large enough radius. Hence, we define the function g as follows

$$g(r) = \frac{r^2}{1 + r^k\theta^{-k}}, \tag{6}$$

that is parameterized with the constant $\theta > 0$ (μm) and exponent $k \geq 2$.

In line with the previous model Soula et al. (2013), adipocyte growth is proportional via parameter α (μm^{-1}.time^{-1}) to a sublinear Michaelian input of extracellular lipids L with constant κ (nmol). Function f is therefore defined as

$$f(L) = \alpha\frac{L}{L + \kappa}. \tag{7}$$

We thus assume that cell size grows when extracellular lipids are available, with a maximal uptake if extracellular lipid amount is large enough.

2.2. Stationary solution

This new model assumes only lipogenic activity. However, we can still derive a stationary cell size distribution and a cell number at equilibrium.

We define $N(t)$ as the total number of cells at time t, e.g.

$$N(t) = \int_{r_{\min}}^{\infty} u(t,s)\mathrm{d}s.$$

By integrating Eq. (1) over r we obtain

$$\int_{r_{\min}}^{\infty} \frac{\partial}{\partial t}u(t,s)\mathrm{d}s + \int_{r_{\min}}^{\infty} \frac{\partial}{\partial r}(V(s,L(t))u(t,s))\mathrm{d}s = -\sigma \int_{r_{\min}}^{\infty} u(t,s)\mathrm{d}s$$

then

$$\frac{d}{dt}\int_{r_{\min}}^{\infty} u(t,s)\mathrm{d}s - V(r_{\min},L(t))u(t,r_{\min}) = -\sigma \int_{r_{\min}}^{\infty} u(t,s)\mathrm{d}s$$

which leads to

$$\frac{dN}{dt}(t) - \rho = -\sigma N(t).$$

From this equation, we derive the number of cells at equilibrium

$$N^\star = \frac{\rho}{\sigma}.$$

We refer to $u^\star$ as a stationary solution of Eq. (1), which satisfies therefore the following equation

$$\frac{d}{dr}\left(V(r,L^\star)u^\star(r)\right) = -\sigma u^\star(r),$$

where $L^\star$ is the stationary amount of extracellular lipids satisfying conservation Eq. (4). Then, since $V(r,L^\star) > 0$ when $r \geq r_{\min}$, we obtain

$$\frac{d}{dr}\left(V(r,L^\star)u^\star(r)\right) = -\frac{\sigma}{V(r,L^\star)}V(r,L^\star)u^\star(r),$$

and then

$$V(r,L^\star)u^\star(r) = \rho \exp\left(-\int_{r_{\min}}^{r} \frac{\sigma}{V(s,L^\star)}\mathrm{d}s\right),$$

where we have used that $V(r_{\min},L^\star)u^\star(r_{\min}) = \rho$.

For clarity, we now add the dependency of L on u (resp. $L^\star$ on $u^\star$) and we obtain the final equation

$$u^\star(r,L^\star) = \frac{\rho}{V(r,L^\star)} \exp\left(-\int_{r_{\min}}^{r} \frac{\sigma}{V(s,L^\star)}\mathrm{d}s\right), \tag{8}$$

yielding a coupled equation with the following equation for $L^\star$, see Eqs. (3)–(4),

$$L^\star = L_0 - \int_{r_{\min}}^{\infty} l(s)u^\star(s,L^\star)\mathrm{d}s. \tag{9}$$

Therefore, $L^\star$ is a fixed point of the following function

$$F(L) = L_0 - \int_{r_{\min}}^{\infty} l(s)u^\star(s,L)\mathrm{d}s, \tag{10}$$

with $u^\star$ given by Eq. (8). When a solution $L^\star$ to Eq. (10) is found, we can insert it into Eq. (8) to obtain the corresponding stationary distribution $u^\star$.

Example 1. *When $g \equiv 1$ is constant and l is given by (5), we obtain the following explicit form for F*

$$F(L) = L_0 - \frac{4\pi}{V_l}\frac{\rho}{\sigma}\frac{f(L)}{\sigma}\left(2\left(\frac{f(L)}{\sigma}\right)^2 + 2r_{\min}\left(\frac{f(L)}{\sigma}\right) + r_{\min}^2\right),$$

which is a continuous and decreasing function of L and thus admits a unique fixed point in $[0, L_0]$ whenever f is increasing with $f(0) = 0$.

Example 1 does not satisfy biological assumptions; it is provided only to illustrate the theory. In Proposition 2, we show that a unique stationary solution exists, generalizing previous example 1 for broader choices of functions l and g, that include biologically-sound choices. Note that even with a simple shape for V, as in Example 1, the solution of Eq. (9) has to be found numerically.

2.3. Parameter estimation

To perform parameter estimation, we set the growth velocity according to Eqs. (6)–(7) so that

$$V(r,L) = \alpha \frac{L}{L+\kappa}\frac{r^2}{1+r^k\theta^{-k}}, \tag{11}$$

with $k \geq 2$. From Eq. (8) the stationary solution is consequently equal to

$$u^\star(r,L^\star) = \rho \frac{L^\star+\kappa}{L^\star}\frac{1+r^k\theta^{-k}}{\alpha r^2}\exp\left(-\frac{\sigma}{\alpha}\frac{L^\star+\kappa}{L^\star}\left[-r^{-1}+r_{\min}^{-1}+\frac{r^{k-1}-r_{\min}^{k-1}}{(k-1)\theta^k}\right]\right). \tag{12}$$

We normalize Eq. (12) to 1 by defining $u^\star_{norm} = \frac{u^\star}{N^\star} = \frac{\sigma u^\star}{\rho}$ and we note $\sigma^\star = \frac{\sigma}{\alpha}\frac{L^\star+\kappa}{L^\star}$ (μm). The previous solution becomes

$$u^\star_{norm}(r,\sigma^\star) = \sigma^\star\left(\frac{1+r^k\theta^{-k}}{r^2}\right)\exp\left(-\sigma^\star\left[-r^{-1}+r_{\min}^{-1}+\frac{r^{k-1}-r_{\min}^{k-1}}{(k-1)\theta^k}\right]\right). \tag{13}$$

From Eq. (13), the solution $u^\star_{norm}$ depends on only 3 parameters: $\sigma^\star$, θ and k. Note that $L^\star$ is now considered as a parameter. Assuming $L^\star$ or L_0 as a parameter is similar. Indeed, by observing distribution of cell sizes $u^\star$ and assuming l to be known (Eq. (5)), $L^\star$ only depends on parameter L_0 from Eq. (9). In addition, we notice that parameter $\sigma^\star$ is a combination of 4 parameters, which cannot be estimated separately by observing $u^\star$.

Parameter estimation is carried out using approximate Bayesian computation (ABC) Toni et al. (2009). We use the ABC rejection sampler algorithm: first we draw a uniform distribution for the 3 parameters of interest, then we compute the L_2 norm of the error between measured and modeled cell size distributions with the drawn parameters. We keep the vector of parameters if the L_2 norm of the error is lower than the chosen threshold and we reject it otherwise. We are considering normalized measured distributions and, for the model we use the explicit formula given by Eq. (13). This procedure is repeated 10^6 times and the threshold is set to $5\,10^{-4}$. The prior uniform distributions for each parameter are the following: $k \sim \mathcal{U}(2.1, 15)$, $\sigma^\star \sim \mathcal{U}(1, 15)$ and $\theta \sim \mathcal{U}(10, 150)$. The algorithm returns the selected parameter vectors. We then compute the average and the standard deviation of each parameter from the selected values.

3. Results

3.1. Proof of existence, uniqueness and stability of the stationary solution

We consider here the following Partial Differential Equation (PDE) problem

$$\begin{cases} \frac{\partial}{\partial t}u(t,r) + \frac{\partial}{\partial r}(V(r,L(t))u(t,r)) = -\sigma u(t,r), & r > r_{\min}, \quad t > 0, \\ V(r_{\min},L(t))u(t,r_{\min}) = \rho, & t > 0, \\ L(t) = L_0 - \int_{r_{\min}}^{\infty} l(s)u(t,s)\mathrm{d}s, & t > 0, \\ u(0,r) = u_0(r), & r > r_{\min}, \end{cases} \tag{14}$$

and we take a general growth velocity under the form

$$V(r,L) = f(L)g(r). \tag{15}$$

To begin with, we study the existence and uniqueness of the stationary solution of system (14) defined by Eq. (8)–(9).

As explained previously, we look for a fixed point of function F defined at Eq. (10). In the following proposition, we prove the existence and uniqueness of the fixed point. Therefore, once L_0 is fixed, there exists a unique value for the stationary extracellular quantity of lipids $L^\star$ and a unique stationary density $u^\star$.

Proposition 2. *We assume that*

- f *is a differentiable strictly increasing function on* $[0, L_0]$ *with* $f(0) = 0$,
- g *is a continuous bounded positive function on* $[r_{\min}, +\infty)$,
- l *is a continuously increasing function on* $[r_{\min}, +\infty)$ *with* $l(r_{\min}) = 0$,
- *for all* $\lambda > 0$, $l/g \in \mathrm{L}^1\big((r_{\min}, +\infty), \exp(-\lambda\chi(x))\mathrm{d}x\big)$, *where* $\chi(x) = \int_{r_{\min}}^{x} \frac{\mathrm{d}s}{g(s)}$.

Then, for all $L_0 > 0$, *there exists a unique fixed point* $L^\star \in (0, L_0)$ *of function* $F : [0, L_0] \to \mathbb{R}$ *defined by*

$$F(L) = L_0 - \int_{r_{\min}}^{\infty} l(s) \frac{\rho}{g(s)f(L)} \exp\left(-\int_{r_{\min}}^{s} \frac{\sigma}{g(\xi)f(L)}\mathrm{d}\xi\right)\mathrm{d}s.$$

Note that functions l, f, g given by (5)–(7)-(6) satisfy the hypotheses of Proposition 2. The proof of Proposition 2 relies on the intermediate value theorem and the fact that F is a decreasing function of L. We will make a repetitive use of the following notation

$$\chi(x) := \int_{r_{\min}}^{x} \frac{1}{g(s)}\mathrm{d}s. \tag{16}$$

By assumption, χ is a diffeomorphism from $[r_{\min}, \infty)$ to $[0, \infty)$ and we define function p by

$$p(x) := l \circ \chi^{-1}(x). \tag{17}$$

Proof. Thanks to notation (16), we can rewrite F as

$$F(L) = L_0 - \frac{\rho}{f(L)} \int_{r_{\min}}^{\infty} \frac{l(s)}{g(s)} \exp\left(-\sigma \frac{\chi(s)}{f(L)}\right)\mathrm{d}s.$$

By assumption and from Lebesgue integration theorem, F is a well defined continuous differentiable function and

- $\lim_{L\to 0} F(L) = L_0$ and
- $\lim_{L\to L_0} F(L) = L_0 - \frac{\rho}{f(L_0)} \int_{r_{\min}}^{\infty} \frac{l(s)}{g(s)} \exp\left(-\sigma \frac{\chi(s)}{f(L_0)}\right)\mathrm{d}s < L_0$.

Thanks to notation (17) and using the change of variable $x = \chi(s)$ in the integral, we obtain

$$F(L) = L_0 - \frac{\rho}{f(L)} \int_{0}^{\infty} p(x) \exp\left(-\sigma \frac{x}{f(L)}\right)\mathrm{d}x.$$

Computing the derivative of F with respect to L, we have that

$$F'(L) = \rho \frac{f'(L)}{f(L)^2} \int_{0}^{\infty} p(x)\left(1 - \sigma \frac{x}{f(L)}\right) \exp\left(-\sigma \frac{x}{f(L)}\right)\mathrm{d}x.$$

By assumption, $f'(L) > 0$ for all $L > 0$, therefore F' has the same sign as the integral $\int_0^\infty p(x)\left(1 - \sigma \frac{x}{f(L)}\right) \exp\left(-\sigma \frac{x}{f(L)}\right)\mathrm{d}x$. We can verify that, for every L,

$$\int_{0}^{\infty} \left(1 - \sigma \frac{x}{f(L)}\right) \exp\left(-\sigma \frac{x}{f(L)}\right)\mathrm{d}x = 0.$$

We can cut the integral above in two parts according to the sign of $1 - \sigma \frac{x}{f(L)}$ and we obtain, using that p is an increasing function, that

$$\begin{aligned}
&\int_{0}^{\infty} p(x)\left(1 - \sigma \frac{x}{f(L)}\right) \exp\left(-\sigma \frac{x}{f(L)}\right)\mathrm{d}x \\
&= \int_{0}^{\frac{f(L)}{\sigma}} p(x)\left(1 - \sigma \frac{x}{f(L)}\right) \exp\left(-\sigma \frac{x}{f(L)}\right)\mathrm{d}x \\
&\qquad + \int_{\frac{f(L)}{\sigma}}^{\infty} p(x)\left(1 - \sigma \frac{x}{f(L)}\right) \exp\left(-\sigma \frac{x}{f(L)}\right)\mathrm{d}x \\
&\le p\left(\frac{f(L)}{\sigma}\right) \int_{0}^{\frac{f(L)}{\sigma}} \left(1 - \sigma \frac{x}{f(L)}\right) \exp\left(-\sigma \frac{x}{f(L)}\right)\mathrm{d}x \\
&\qquad + p\left(\frac{f(L)}{\sigma}\right) \int_{\frac{f(L)}{\sigma}}^{\infty} \left(1 - \sigma \frac{x}{f(L)}\right) \exp\left(-\sigma \frac{x}{f(L)}\right)\mathrm{d}x \\
&\le p\left(\frac{f(L)}{\sigma}\right) \int_{0}^{\infty} \left(1 - \sigma \frac{x}{f(L)}\right) \exp\left(-\sigma \frac{x}{f(L)}\right)\mathrm{d}x = 0.
\end{aligned}$$

We deduce that $F'(L) \le 0$, consequently F is continuous nonincreasing. Since $F(0) > 0$ and $F(L_0) < L_0$, F has a unique fixed point $L^* \in (0, L_0)$. □

Now, we prove that the unique stationary solution we found is locally stable for PDE system (14). Thus, the stationary solution represents the asymptotic profile of the system, provided that the initial datum is close to the stationary solution.

Theorem 3. *We assume that:*

(H1) $f \in C^1([0, L_0])$ *is strictly increasing and* $f(0) = 0$.
(H2) $g \in C^1([r_{\min}, +\infty))$, $g > 0$ *and* g *and* g' *are bounded.*
(H3) $l \in C^1([r_{\min}, +\infty))$, l *is increasing with* $l(r_{\min}) = 0$ *and* $\frac{l'}{1+l}$ *is bounded. Furthermore, there exist* $x_0 > 0$ *and* $K > 0$ *such that for all* $x, y \ge x_0$, $l(x + y) \le K l(x) l(y)$.
(H4) For all $\lambda > 0$, *both* l/g *and* l' *belong to* $\mathrm{L}^1((r_{\min}, +\infty), (\exp(-\lambda\chi(x))\mathrm{d}x)$.

Then the unique stationary solution of system (14) *is locally asymptotically stable in the space* $\mathrm{L}^1\big((r_{\min}, +\infty), (1 + l(x))\mathrm{d}x\big)$.

Functions f, g, l given by (7)–(6)–(5) satisfy the hypotheses. We sketch here the general idea of the proof, all the details and intermediate computations are given in Appendix A.

Proof. Thanks to the separable form of the growth speed $V(r, L) = f(L)g(r)$ and using the change of variable $v(\tau, \cdot) = u(t, \cdot)$ with $\tau(t) = \int_0^t f(L(\theta))\mathrm{d}\theta$, we can show that the PDE system (14) is asymptotically equivalent to the following semilinear PDE

$$\begin{cases}
\frac{\partial}{\partial\tau} v(\tau, r) + \frac{\partial}{\partial r}(g(r)v(\tau, r)) + \frac{\sigma}{f(L(\tau))} v(\tau, r) = 0, & r > r_{\min}, \tau > 0, \\
g(r_{\min}) f(L(\tau)) v(\tau, r_{\min}) = \rho, & \tau > 0, \\
L(\tau) = L_0 - \int_{r_{\min}}^{\infty} l(r) v(\tau, r)\mathrm{d}r, & \tau > 0, \\
v(0, r) = u_0(r), & r > r_{\min}.
\end{cases} \tag{18}$$

Eq. (18) can be rewritten as an abstract semilinear Cauchy problem on the Banach space $X := \mathbb{R} \times \mathrm{L}^1((0, +\infty), \omega(x)\mathrm{d}x)$ for some suitable weight function ω. Then, the principle of linearized stability (Prop. 5.7.1. and 5.7.4. in Magal and Ruan (2018)) allows us to reduce the stability analysis to the study of the asymptotic behavior of the linearized problem around the stationary solution. The study of the linearized problem around $(u^\star, L^\star)$, leads to consider the following characteristic function Δ (see the derivation of Δ in Appendix A).

$$\Delta(\lambda) = 1 + \rho \frac{f'(L^\star)}{f^2(L^\star)} \frac{1}{\lambda} \int_{0}^{\infty} p(x) e^{-\frac{\sigma}{f(L^\star)}x} \left(\frac{\sigma}{f(L^\star)} - e^{-\lambda x}\left(\lambda + \frac{\sigma}{f(L^\star)}\right)\right)\mathrm{d}x,$$

where we recall that p is defined at Eqs. (16)–(17). It remains to show that the characteristic function Δ has no root with non-negative real part, which implies that the unique stationary solution of system (14) is locally asymptotically stable. Let us remark that $\lambda \neq 0$ and $\Delta(\lambda) = 0$ is equivalent to

$$\lambda = \rho \frac{f'(L^\star)}{f^2(L^\star)} \int_{0}^{\infty} p(x) e^{-\frac{\sigma}{f(L^\star)}x} \left(e^{-\lambda x}\left(\lambda + \frac{\sigma}{f(L^\star)}\right) - \frac{\sigma}{f(L^\star)}\right)\mathrm{d}x. \tag{19}$$

For the sake of brevity, we set $\lambda_0 := \frac{\sigma}{f(L^\star)}$. Then Eq. (19) can be rewritten as

$$\begin{aligned}
\frac{f^2(L^\star)}{\rho f'(L^\star)} \lambda &= \int_{0}^{\infty} p(x) e^{-\lambda_0 x}\left(e^{-\lambda x}(\lambda + \lambda_0) - \lambda_0\right)\mathrm{d}x \\
&= \int_{0}^{\infty} p(x) e^{-(\lambda_0 + \lambda)x}(\lambda + \lambda_0)\mathrm{d}x - \lambda_0 \int_{0}^{\infty} p(x) e^{-\lambda_0 x}\mathrm{d}x.
\end{aligned}$$

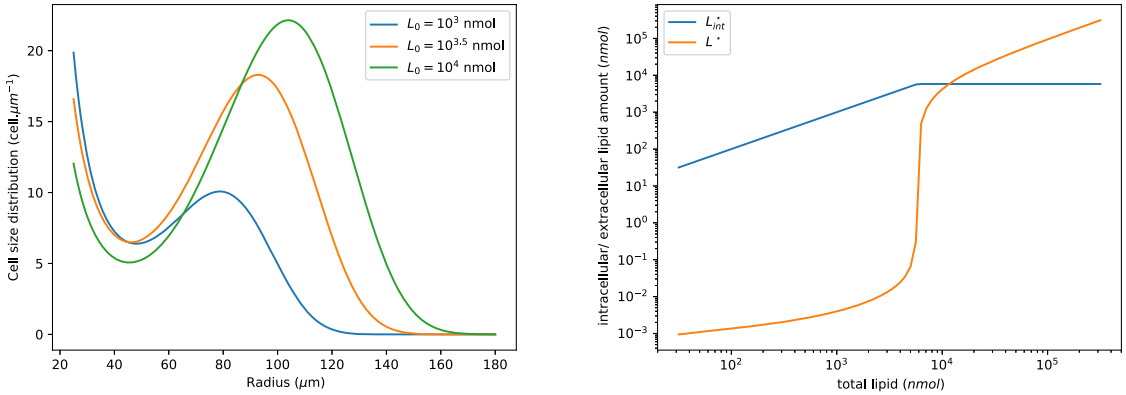

Fig. 1. Effect of total lipid quantity on stationary solution. Left panel: plot of stationary solution (9)-(12) for three values of L_0 (to obtain visually comparable graphs radii r start at 25μm). Right panel: log-log plot of the extracellular lipid amount $L^\star$ (orange) and intracellular lipid amount $L^\star_{\text{int}}$ (blue) with respect to L_0. Parameters are: $V_l = 1.091.10^6 \mu m^3.\text{nmol}^{-1}$, $\alpha = 10^{-4} \mu m^{-1}.\text{time}^{-1}$, $\theta = 50\mu$m, $\sigma = 5.10^{-4}$ time^{-1}, $\rho = 1$ cell.time^{-1}, $k = 6$, $\kappa = 10^{-2}$ nmol, $r_{\min} = 10\mu$m.

By integration by parts and using that $p(0) = 0$ by (H3), we get

$$\frac{f^2(L^\star)}{\rho f'(L^\star)}\lambda = \int_0^\infty p'(x)e^{-(\lambda_0+\lambda)x}\mathrm{d}x - \int_0^\infty p'(x)e^{-\lambda_0 x}\mathrm{d}x$$
$$= \int_0^\infty p'(x)e^{-\lambda_0 x}\left(e^{-\lambda x} - 1\right)\mathrm{d}x.$$

Using the complex decomposition of $\lambda = \Re(\lambda) + i\Im(\lambda)$ and taking the real part of the later equation, we obtain

$$\frac{f^2(L^\star)}{\rho f'(L^\star)}\Re(\lambda) = \int_0^\infty p'(x)e^{-\lambda_0 x}\left(\cos(\Im(\lambda)x)e^{-\Re(\lambda)x} - 1\right)\mathrm{d}x.$$

From (H1), since $L^\star \neq 0$, we have $\dfrac{f^2(L^\star)}{\rho f'(L^\star)} > 0$. If $\Re(\lambda) > 0$, by $(H2)$ and $(H3)$, p is increasing, thus we get

$$\int_0^\infty p'(x)e^{-\lambda_0 x}\left(\cos(\Im(\lambda)x)e^{-\Re(\lambda)x} - 1\right)\mathrm{d}x \leq 0, \tag{20}$$

leading to a contradiction. If $\Re(\lambda) = 0$, the equation above leads to $\Im(\lambda) = 0$ which is impossible since $\lambda \neq 0$. Therefore, Δ has no root with non-negative real part and we can conclude to the local asymptotic stability of the stationary solution. □

3.2. Numerical simulation

We perform several numerical experiments, using the model under consideration with functions l, f, g given by (5)–(7)–(6). First, we explore the effect of the total lipid quantity L_0 by computing the stationary solution defined by the solution of the coupled Eqs. (9)–(12). In the left panel of Fig. 1, we represent cell size distributions for three values of L_0. To be able to compare the different graphs, we start the radius value at 25 μm in the plots. An increase in total amount of lipids L_0 increases the lipid volume inside cells, and the distribution of cell sizes remains bimodal.

We also show the allocation of lipids between the cells and the extracellular medium. The stationary amount of intracellular lipids is defined by $L^\star_{\text{int}} := \int_{r_{\min}}^\infty \frac{4\pi}{3V_l}(s^3 - r_{\min}^3)u^\star(s)\mathrm{d}s$, see Eq. (3) and (5). Fig. 1 right panel displays a log-log plot of the stationary extracellular lipids $L^\star$ and stationary intracellular lipids $L^\star_{\text{int}}$ as a function of L_0. For low values of L_0, $L^\star$ is small and almost constant, and we find that the uptake of lipids by the cells $L^\star_{\text{int}}$ increases proportionally to the amount of available lipid L_0 (a linear regression in a log-log plot gives a regression coefficient close to 1). Above a certain value of L_0, a plateau is reached for the intracellular lipid amount $L^\star_{\text{int}}$, corresponding to the maximal lipid amount the tissue can store. For values above this threshold of L_0, the intracellular lipids stop increasing and the extracellular lipids start to accumulate, i.e. $L^\star$ increases sharply.

We will perform in Section 3.3 a data fitting procedure using the normalized stationary solution (13) to estimate 3 parameters: k, θ and $\sigma^\star$. First, Fig. 2 shows the effect of varying these 3 parameters on the shape of the normalized stationary solution. Fig. 2 top left panel shows that coefficient k mostly impacts the right mode of the cell size distribution, namely the large-size mode. It plays a role on both the position and the height of this mode. For the chosen parameters, we notice that $k = 3$ is not sufficient to obtain bimodality of the distribution. Fig. 2 top right panel shows the influence of parameter θ on the cell size distribution. Similarly to k, it impacts the position and height of the right mode. We can say that parameter θ mostly represents the nadir, that is to say, the lowest point between the two modes, of the cell size distribution. Finally, Fig. 2 bottom left panel shows the dependency with respect to $\sigma^\star$. This parameter has a huge overall impact on the distribution since $\sigma^\star$ corresponds to the ratio between the cell death rate σ and the growth rate coefficient $\alpha\frac{L^\star}{L^\star+\kappa}$. Parameter $\sigma^\star$ affects both small and large size frequencies.

3.3. Comparison between modeled and measured cell size distributions

A general fitting approach is not the goal of this article. Instead, we want to assess if this new model produces accurate cell size distributions. We randomly select four adipose size distributions from our database, which contains retro-peritoneal adipose tissues of male Wistar rats from different experiments Jacquier et al. (2014), Soula et al. (2015). The code and the data files to perform the estimations are available here: https://plmlab.math.cnrs.fr/audebert/adipocyte_rapid_turnover_modeling.

The ABC rejection sampler algorithm is applied to each data set. The selection rates are low, as expected with this method Toni et al. (2009) and the number of selected parameter vectors varies from 52 to 1524. The posterior distributions have a Gaussian shape and are far from the bounds of the prior uniform distributions, see Sup. Fig. B.5. The estimated parameters are chosen as the mean of the selected list of parameters and we also compute their standard deviation. Table 1

Table 1
Estimations obtained with ABC rejection sampler for each animal. The mean and standard deviation of the selected list of parameters are presented for each animal. The procedure is repeated 10^6 times and the threshold is set to $5\,10^{-4}$.

animal	$\sigma^\star$ (μm)	θ (μm)	k
rat 1	6.24 ± 0.6	33.7 ± 2.15	6.08 ± 0.7
rat 2	7.58 ± 0.81	30.33 ± 4.37	3.82 ± 0.72
rat 3	5.28 ± 0.24	43.07 ± 0.78	9.26 ± 0.38
rat 4	6.03 ± 0.73	42.87 ± 3.09	7.55 ± 1.06

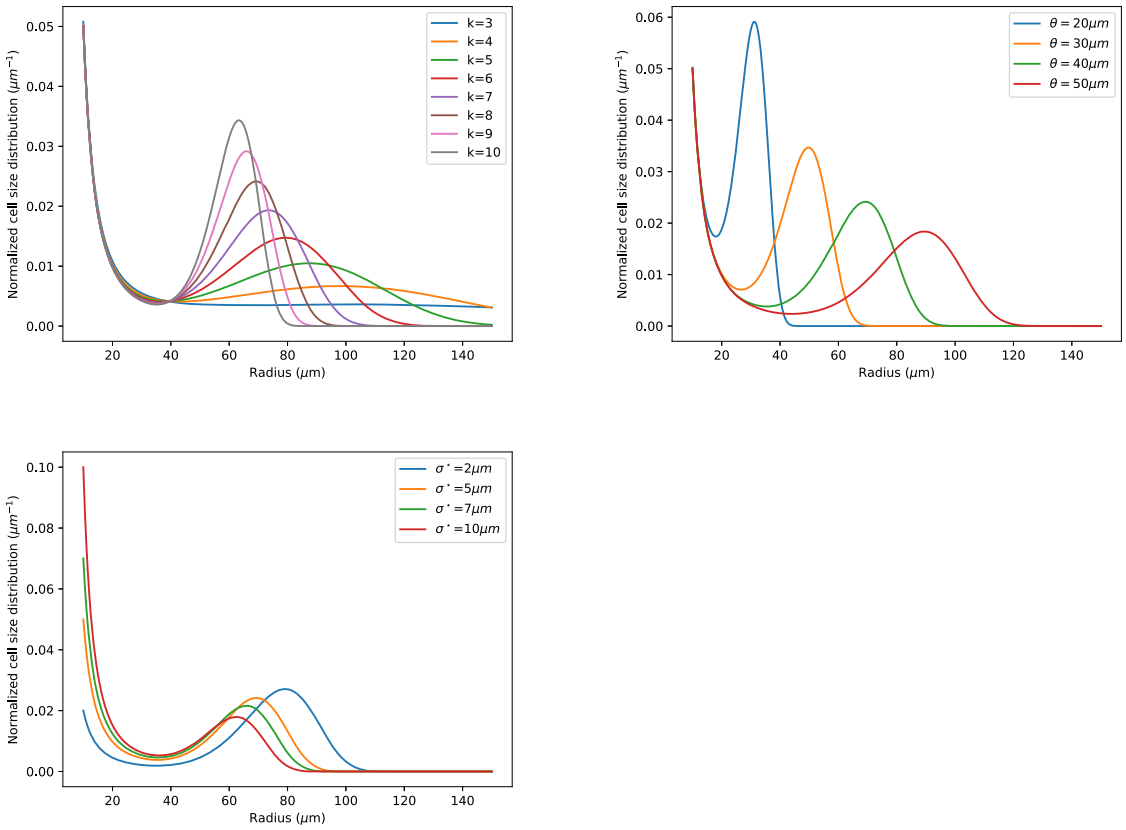

Fig. 2. Sensitivity of stationary solution defined in Eq. (13) to the 3 parameters. Top left: dependency of the stationary solution with respect to parameter k. Top right: impact of θ parameter on the stationary solution. Bottom left: impact of $\sigma^\star$ parameter on the stationary solution. Default parameters are: $k = 8$, $\theta = 40\mu$m, $\sigma^\star = 5\mu$m, $r_{\min} = 10\mu$m.

presents the estimated values for the four animals. The small standard deviations show the robustness of the parameter estimation. In addition, the estimated parameters do not vary wildly between data sets. Fig. 3 shows that the model is in good agreement with measured adipocyte size distributions.

Considering that adipocyte death follows a linear decay with parameter σ in Eq. (1), individual adipocyte turnover time is on average equal to $1/\sigma$. We know from literature that 0.6 % to 1.5 % adipocytes are replaced each day for lean mice ad libitum Rigamonti et al. (2011), Neese et al. (2002), Kim et al. (2014). This corresponds to a turnover ranging from 45 days to 115 days. Those estimations enable us to fix the time unit to day in the model, although before it was an arbitrary time unit. From the estimated values for $\sigma^\star$, see Table 1, we can compute an estimation of the velocity rate $\alpha^\star$ defined by

$$\alpha^\star = \alpha \frac{L^\star}{L^\star + \kappa} = \frac{\sigma}{\sigma^\star}\ \mu\text{m}^{-1}.\text{day}^{-1}.$$

Under these assumptions, lower ($\alpha^\star_{115}$) and upper ($\alpha^\star_{45}$) bounds for the rate $\alpha^\star$ can be estimated for each rat. These estimations are presented in Table 2. From the estimation of $\alpha^\star$ we can also compute lower and upper bounds for the velocities with respect to radius, thanks to Eq. (11). Left panel of Fig. 4 shows the velocity for rat 4 assuming 45 or 115 days for adipocyte turnover. For 45 days turnover, the velocity increases faster and higher with respect to radius. In addition, we compute the averaged velocity $\bar{V} = \int_{r_{\min}}^{r_{\max}} V(x) u^\star_{norm}(x) dx$ with lower and upper bounds for $\alpha^\star$ and the estimated parameters for each animal, see Table 2. Under our assumptions, the velocity ranges from 0.28 to 0.92 μm.day^{-1}. Right panel of Fig. 4 shows, for rat 4, the trajectory of two cells with initial radius of 10 μm, one with the highest estimated velocity and the other with the lowest estimated velocity. The displayed dots represent the cell radius after $1/\sigma$, $2/\sigma$ and $3/\sigma$ days in both cases. Since turnover time is on average equal to $1/\sigma$, it is likely that the adipocyte dies after reaching the first displayed dot. A rapid increase in size is observed for the upper velocity bound, followed by a plateau. The cell with the lower bound velocity shows similar dynamics with a smaller velocity and ends with a lower size.

Table 2
Lipid uptake rate and average velocity for each animal. Parameter $\alpha^\star$ and average velocity ($\int_{r_{\min}}^{r_{\max}} V(x) u^\star_{norm}(x) dx$) are computed with estimations from literature for $1/\sigma$ and ABC rejection algorithm for the other parameters (Table 1). The subscript $_{.115}$ corresponds to the computation for a turnover of 115 days and $_{.45}$ for a turnover of 45 days.

animal	$\alpha^\star_{115}$ (μm^{-1}.day^{-1})	$\bar{V}_{115}$ (μm.day^{-1})	$\alpha^\star_{45}$ (μm^{-1}.day^{-1})	$\bar{V}_{45}$ (μm.day^{-1})
rat 1	0.0014	0.2897	0.0036	0.7403
rat 2	0.0011	0.2859	0.0029	0.7308
rat 3	0.0016	0.3537	0.0042	0.9039
rat 4	0.0014	0.3585	0.0037	0.9162

4. Discussion

In this paper, we provide a new dynamical model for the time evolution of adipocyte size distributions. In this model, cells are constantly growing in size and they tend to accumulate at sizes where growth velocity is low. This can be compared to a "toll effect", when toll gate slows down cars, leading to an increase of local density. The growth velocity is tailored to obtain the desired shape for cell size distributions. However, we stress that the growth rate remains biologically plausible. Indeed, for small radii, the growth velocity is proportional to the cell surface Soula et al. (2015), Gliemann and Vinten (1974), Smith (1971). The growth rate then increases and reaches a maximum for an intermediate size around the nadir. For larger radii, the tissue prevents the cell growth,

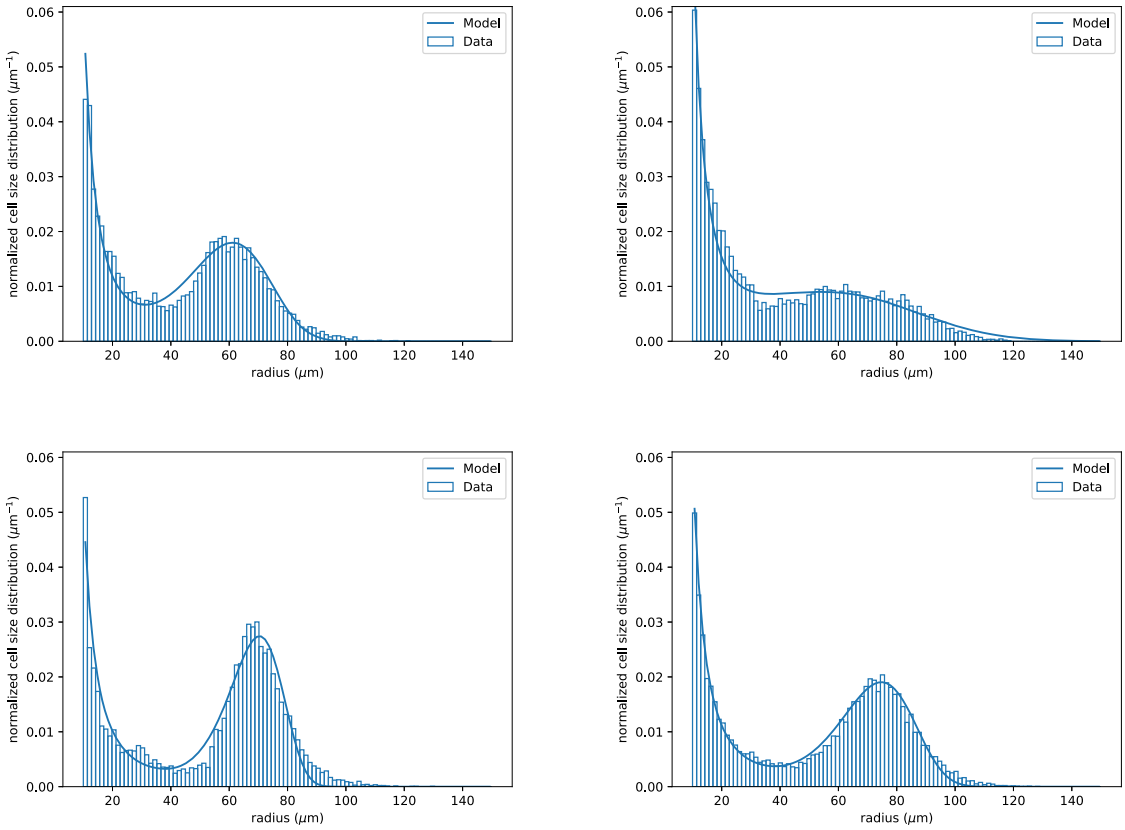

Fig. 3. Model compared to measurements for cell size distributions of four different male Wistar rats Jacquier et al. (2014), Soula et al. (2015). Table 1 presents the estimated parameters and the model is described by Eq. (13). Data are represented with histograms and the model output with solid lines.

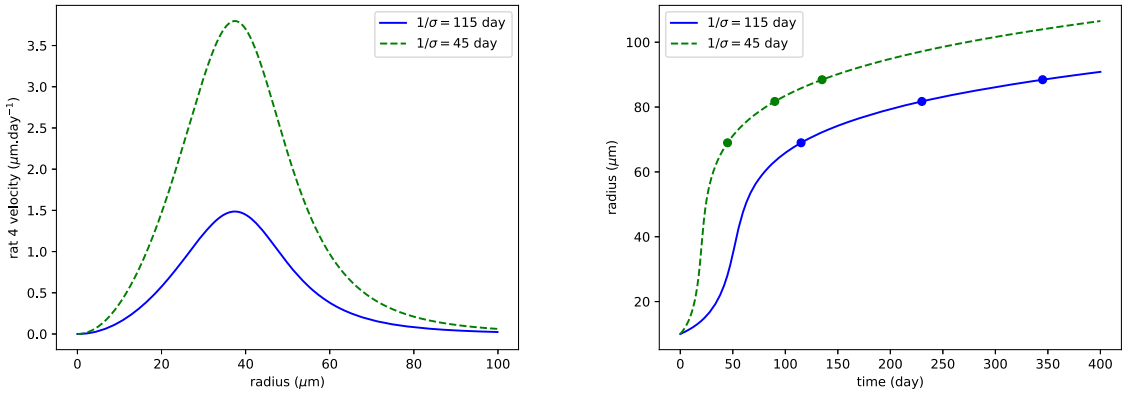

Fig. 4. Example of velocity functions V and cell radius trajectories. Left panel shows velocity functions (Eq. (11)) with respect to radius computed for two different turnover times and with the estimated parameter values of rat 4 (Tables 1 and 2). Right panel shows cell trajectory with velocity estimated for rat 4 with 45 and 115 days for adipocyte turnover. Initially $r(0) = 10\,\mu$m and the curve is computed with explicit Euler scheme $r_{k+1} = r_k + dtV(r_k)$ and $dt = 0.01$ day. Dots point out the cell radius after $1/\sigma$, $2/\sigma$ and $3/\sigma$ days in each case.

and growth velocity decreases towards zero. The resulting cell size distribution yields a bimodal distribution, i.e., cell accumulation around the sizes of low growth rates both for small and large enough radii. The death term prevents accumulation of cells at sizes larger than the physiological limit. These model assumptions are different from the models we proposed previously Soula et al. (2013, 2015), Meyer et al. (2024), Giacobbi et al. (2024), Dauger et al. (2025). In these former models, the growth velocity describes lipid exchanges. The two modes of the stationary solution correspond to the equilibria between lipogenesis and lipolysis, that is to say, the zeroes of the growth velocity. To conclude, with a constant inflow of cells, constant cell death, and continuous cell growth we can obtain extremely realistic adipocyte size distributions.

We prove that the proposed model admits a unique stationary solution, that is locally asymptotically stable, for a broad class of functional forms. This justifies the data fitting procedure with the stationary solution. The key assumption that enables the study of the long-time behavior of the model is the separability of the adipocyte growth rate into two distinct functions: one depending only on the extracellular lipid amount, and the other only on the cell radius. The mathematical analysis of the long-term behavior of general size-structured population models is known to be particularly challenging. However, when the growth rate has a separable form, an implicit time-rescaling transformation can be employed to eliminate the nonlinearity in the growth rate. This transformation allows us to rewrite the model as a semilinear abstract Cauchy

problem, to which well-established stability results can be applied Magal and Ruan (2018). To our knowledge, this strategy has been successfully applied in the context of erythropoiesis modeling Grabosch and Heijmans (1990, 1991), and oogenesis modeling Clément et al. (2024). In our context, in addition to the separability assumption, the existence of a unique locally stable steady state mainly relies on two biologically natural assumptions: (i) adipocytes grow faster when more extracellular lipids are available, and (ii) the amount of lipids stored in an adipocyte increases with its size.

The measured, and simulated cell size distributions are in good agreement. The proposed model reproduces most of the distribution features, i.e. the bimodal shape, the overall size range, and the increase of the large-size mode with higher lipid input. With this model, the adipose tissue presents a maximum storage capacity beyond which the extracellular lipids accumulate, similarly to former models Soula et al. (2013), Dauger et al. (2025).

However, our modeling assumptions present some limitations. The death rate is constant, and does not depend on cell size, which might be unrealistic, in diet change for example. Increased death rate has been associated with increased adipocyte size and, in obesity, an increased turnover has been reported Cinti et al. (2005), Han et al. (2025). For instance, in Jo et al. (2010), a death rate has been considered only for cells above a critical size. This death rate was found in agreement with the decrease of total adipose cell number under 19 weeks of high-fat diet. Different death rates could be taken into account as extensions of the model presented in this article, but the death rate should be selected with respect to the longitudinal study under consideration.

Moreover, we only consider in our model a recruitment of new adipocytes which is constant in time. Constant rates for cell recruitment, and cell death are needed to obtain the existence of a stationary solution, and to compute it. Studying cell size dynamics, a constant recruitment rate holds only if the rate variation can be neglected over the total time period that is studied. This assumption has already been made in previous models for cell size distribution dynamics Jo et al. (2009, 2010, 2012). In addition, what is called recruitment rate here is actually a sum of several biological processes. New adipocytes come from the differentiation of pre-adipocyte cells. This differentiation is the result of sequential activation of transcription factors Sethi and Vidal-Puig (2007), and also depends on hormones, like insulin. An individual-based and multiscale framework Bernard (2013) would be necessary to take into account such signaling cascades. In terms of dynamics, no clear connection between an increase of the number of adipocytes and a growth of their size is known Spalding et al. (2008). The computation of model solution may be challenging under the assumption that the recruitment of adipocytes is varying with time, with extracellular lipids or with intracellular lipids. However, it may enable the exploration of the trade-off between hyperplasia, i.e. increase of cell numbers, and hypertrophy, i.e. increase of cell sizes, to manage lipid storage Sakers et al. (2022); it is foreseen to consider the case of varying in time recruitment rate in further works.

Until now, we have worked with stationary distributions, assuming the data are at equilibrium. Time dependent variables will allow us to study non-stationnay solutions in order to mimic for example dietary changes and food input imbalance. Time dynamics may enable us to choose between different assumptions on new adipocyte recruitment or cell death. In addition, the role of extracellular lipids, and their evolution over time would be important. One may try to control this quantity to avoid lipotoxicity. When fat mass increases drastically, the adipose tissue experiences remodeling, especially the extracellular matrix. These modifications lead to the accumulation of collagen fibers in the tissue, that is to say fibrosis. Fibrosis has been associated with metabolic and adipocyte growth disorders Divoux and Clément (2011). To our knowledge, no mathematical model has considered fibrosis formation within adipocyte tissues until now. Taking into account fibrosis in future mathematical models of adipose tissue is one of the challenges that remain to be tackled.

Unlike our previous models, this model links the age (time since recruitment) of the cells and their size. This direct link is due to the constant recruitment of new cells at minimal size and the constantly growing in size assumptions. It leads to larger cells being “older” than smaller cells. Whether the adipocyte size is related to its age could certainly be tested with real experiments. This would enable to establish if adipocyte size and age are related or not.

One of the true advantages of the proposed model is the explicit form for a normalized stationary solution, that is parameterized by three parameters. The fit with the three parameter function is robust and well-posed, in the sense that a fit will lead to a unique set of parameters. In addition, one of the parameters, the parameter θ, automatically gives an estimate of the distribution nadir. We perform an ABC rejection algorithm that can be computationally costly if the cost function is slow to compute. Here, with the explicit form of $u^{\star}_{norm}$ given by Eq. (13), the estimation computations are very fast. This explicit function gives a new way to fit adipocyte size distributions with only three parameters. In past works, distributions of adipocyte sizes have been fitted with two exponential functions and a Gaussian, yielding at least six parameters McLaughlin et al. (2007), Jo et al. (2009), Soula et al. (2015).

This model presents a novel, and simple view of the adipocyte size distribution as a stationary distribution of ever growing, albeit dying, cells. In accordance with our previous models, it does not suppose any cell subpopulations, and does not need any individual cell variation Soula et al. (2013), Dauger et al. (2025) or diffusion term Giacobbi et al. (2024), Meyer et al. (2024) to reproduce measured distributions.

CRediT authorship contribution statement

Louis Fostier: Writing – original draft, Methodology, Formal analysis; **Aloïs Dauger:** Writing – original draft; **Romain Yvinec:** Writing – review & editing, Supervision, Methodology, Conceptualization; **Magali Ribot:** Writing – review & editing, Supervision, Methodology, Conceptualization; **Chloe Audebert:** Writing – review & editing, Validation, Supervision, Software, Project administration, Methodology; **Hedi Soula:** Writing – review & editing, Writing – original draft, Validation, Supervision, Software, Methodology, Conceptualization.

Declaration of competing interest

The authors declare that they have no known competing financial interests or personal relationships that could have appeared to influence the work reported in this paper.

Acknowledgments

The authors acknowledge the support of the French Agence Nationale de la Recherche (ANR), under MATIDY grant ANR-20-CE45-0003-01.

Appendix A. Proof of Theorem 3.

We will first show that system of Equation (18) can be written as an abstract non-densely defined semilinear Cauchy problem on the Banach space $X := \mathbb{R} \times \mathrm{L}^1((0,+\infty), \omega(x)\mathrm{d}x)$ for some suitable weight function ω. Then, the principle of linearized stability, stated in Magal and Ruan (2018) (see Prop. 5.7.1. and Prop. 5.7.4.) for these problems, allows us to reduce the stability analysis to the study of the asymptotic behavior of the linearized problem around the stationary solution, under some regularity hypotheses on the model parameters. We then study the asymptotic behavior of the linearized problem thanks to arguments from linear semigroup theory.

For the reader’s convenience, we recall here the assumptions (H1)-(H4) of Theorem 3:

(H1) $f \in C^1([0, L_0])$ is strictly increasing and $f(0) = 0$,

(H2) $g \in C^1([r_{\min}, +\infty))$, $g > 0$ and g and g' are bounded,

(H3) $l \in C^1([r_{\min}, +\infty))$, l is increasing with $l(r_{\min}) = 0$ and $\frac{l'}{1+l}$ is bounded. Furthermore, there exist $x_0 > 0$ and $K > 0$ such that for all $x, y \geq x_0$, $l(x+y) \leq K l(x) l(y)$,

(H4) for all $\lambda > 0$, both l/g and l' belong to $\mathrm{L}^1((r_{\min}, +\infty), (\exp(-\lambda\chi(x))\mathrm{d}x)$.

From Proposition 2, we know that $L^\star > 0$. Let $\varepsilon > 0$ such that $L^\star > \varepsilon$. As we consider the local stability of the stationary solution, we can replace f by a function $\tilde{f}$ defined on $\mathbb{R}$ such that $\tilde{f} \geq f(\varepsilon/2) > 0$, $\tilde{f} \in C^1(\mathbb{R})$ and $f \equiv \tilde{f}$ on $[\varepsilon, +\infty)$. This trick does not change the stationary solution nor its local stability and it simplifies the formalization of the abstract Cauchy problem. In what follows, $\tilde{f}$ is denoted by f to ease the notation.

With arguments similar to those in Section 3 of Clément et al. (2024), we can check that the stationary solution $v^\star$ of system (18) is equal to the stationary solution $u^\star$ of system (14). As f is a differentiable strictly increasing function on $[0, L_0]$, we can verify that the local $\mathrm{L}^1((r_{\min}, +\infty), (1 + l(x))\mathrm{d}x)$-stability (resp. local asymptotic stability) of $u^\star$ is equivalent to the local $\mathrm{L}^1((r_{\min}, +\infty), (1 + l(x))\mathrm{d}x)$-stability (resp.local asymptotic stability) of $v^\star$. This time-scaling transformation removes the nonlinear part of the growth rate, so that the long-time behavior of system (14) can be studied using results from semilinear equation theory.

As g is positive, we can also perform the following change of space variable

$$x = \chi(r) := \int_{r_{\min}}^{r} \frac{1}{g(s)} \mathrm{d}s \tag{A.1}$$

and $w(\tau, x) = v(\tau, r)$, which leads to a system with a growth rate constant equal to 1. Indeed, we obtain the following system for w

$$\begin{cases} L(\tau) = L_0 - \int_0^\infty k(x) w(\tau, x)\mathrm{d}x, & \tau > 0, \\ \partial_\tau w(\tau, x) + \partial_x w(\tau, x) + \left(m(x) + \frac{\sigma}{f(L(\tau))}\right) w(\tau, x) = 0, & x > 0, \tau > 0, \\ g(r_{\min}) f(L(\tau)) w(\tau, 0) = \rho, & \tau > 0, \\ w(0, x) = w_0(x), & x > 0, \end{cases} \tag{A.2}$$

where $m = g' \circ \chi^{-1}$, $w_0 = u_0 \circ \chi^{-1}$ and $k = (l \circ \chi^{-1}) \times (g \circ \chi^{-1})$. Then, the local $\mathrm{L}^1((r_{\min}, +\infty), (1 + l(x))\mathrm{d}x)$-stability (resp. local asymptotic stability) of $u^\star$ is equivalent to the local $\mathrm{L}^1((0, +\infty), \omega(x)\mathrm{d}x)$-stability (resp. local asymptotic stability) of $w^\star$, the stationary solution of system (A.2), given by $w^\star = u^\star \circ \chi^{-1}$. Here, the weight ω is defined by

$$\omega := g(1 + l) \circ \chi^{-1}. \tag{A.3}$$

We consider the Banach space $X := \mathbb{R} \times \mathrm{L}^1((0, +\infty), \omega(x)\mathrm{d}x)$ endowed with the norm

$$\left\| \begin{pmatrix} a \\ \psi \end{pmatrix} \right\|_X := |a| + \frac{1}{\omega(0)} \|\phi\|_{\mathrm{L}^1((0,+\infty),\omega(x)\mathrm{d}x)} = |a| + \frac{1}{\omega(0)} \int_0^\infty \omega(x)|\phi(x)|\mathrm{d}x. \tag{A.4}$$

Remark that, by (H4) and Eq. (8), $u^\star \in \mathrm{L}^1((r_{\min}, +\infty), (1 + l(x))\mathrm{d}x)$, so that $w^\star \in L^1((0, +\infty), \omega(x)dx)$ and $(0, w^\star) \in X$.

Let us define the following linear operator $A : D(A) \subset X \to X$ by

$$A \begin{pmatrix} 0 \\ \phi \end{pmatrix} = \begin{pmatrix} -\phi(0) \\ -\partial_x \phi \end{pmatrix}, \quad D(A) = \{0\} \times \left(\mathrm{L}^1((0, +\infty), \omega(x)\mathrm{d}x) \cap W^{1,1}((0, +\infty), \mathrm{d}x)\right) \tag{A.5}$$

and the map $G : \overline{D(A)} = \{0\} \times \mathrm{L}^1((0, +\infty), \omega(x)\mathrm{d}x) \to X$ by

$$G \begin{pmatrix} 0 \\ \phi \end{pmatrix} = \begin{pmatrix} R(\phi) \\ M(\phi) \end{pmatrix},$$

with

$$R(\phi) := \frac{\rho}{g(r_{\min}) f(L_0 - \int_0^\infty k(x)\phi(x)\mathrm{d}x)}$$

and

$$M(\phi) = -m\phi - \frac{\sigma}{f(L_0 - \int_0^\infty k(x)\phi(x)\mathrm{d}x)} \phi.$$

Then, system (A.2) can be written as the following semilinear abstract Cauchy problem

$$\begin{cases} \frac{d\mathbf{w}}{d\tau}(\tau) = A\mathbf{w}(\tau) + G(\mathbf{w}(\tau)), & \tau > 0, \\ \mathbf{w}(0) = \begin{pmatrix} 0 \\ w_0 \end{pmatrix} \in \overline{D(A)}, \end{cases} \tag{A.6}$$

with $\mathbf{w} = \begin{pmatrix} 0 \\ w \end{pmatrix}$. A is a linear operator with a non-dense domain in X (i.e., $\overline{D(A)} \neq X$). Therefore, for any linear operator $L \in \mathcal{L}(X)$, we consider its restriction to $\overline{D(A)}$, denoted by $L_{\overline{D(A)}}$ and defined by:

$$L_{\overline{D(A)}} : D(L_{\overline{D(A)}}) \subset \overline{D(A)} \to \overline{D(A)}, \quad L_{\overline{D(A)}} x := Lx,$$

for all $x \in D(L_{\overline{D(A)}}) := \{x \in D(L) \cap \overline{D(A)} \mid Lx \in \overline{D(A)}\}$. The map G is continuously differentiable around stationary solution $\mathbf{w}^\star = \begin{pmatrix} 0 \\ w^\star \end{pmatrix}$ and the linearized problem around $\mathbf{w}^\star$ is given by

$$\frac{d\mathbf{w}}{d\tau}(\tau) = A\mathbf{w}(\tau) + DG(\mathbf{w}^\star)\mathbf{w}(\tau), \ \tau \geq 0, \ \mathbf{w}(0) = \mathbf{w_0} \in \overline{D(A)}.$$

Here $DG(\mathbf{w}^\star) \in \mathcal{L}(\overline{D(A)}, X)$ is the Fréchet derivative of G at $\mathbf{w}^\star$ and is given explicitly as

$$DG(\mathbf{w}^\star) \begin{pmatrix} 0 \\ \phi \end{pmatrix} = \begin{pmatrix} \frac{\rho}{g(r_{\min})} \frac{f'(L^\star)}{f(L^\star)^2} \int_0^\infty k(x)\phi(x)\mathrm{d}x \\ \left(-\sigma \frac{f'(L^\star)}{f(L^\star)^2} \int_0^\infty k(x)\phi(x)\mathrm{d}x\right) w^\star - \left(\frac{\sigma}{f(L^\star)} + m\right)\phi \end{pmatrix}, \tag{A.7}$$

with $L^* = L_0 - \int_0^\infty k(x) w^*(x) dx$.

The following proposition is crucial. Indeed, the Hille–Yosida property of the linear operator A allows us to apply the principle of linearized stability, namely to verify the assumptions of Prop. 5.7.1 and 5.7.4 of Magal and Ruan (2018). Moreover, the negativity of the essential growth bound of the linearized operator enables us to study the asymptotic behavior of the linearized problem. To do so, we analyze the spectral bound of the associated operator, as justified by Corollary IV.2.11 in Engel and Nagel (2000), similarly to what is done in finite-dimensional dynamical systems.

Proposition 4. *Let assumptions $(H1) - (H4)$ hold. Then A defined by (A.5) is a closed Hille-Yosida operator. Furthermore, let $\mathbf{w}^\star$ be a stationary solution of Eq. (A.6), then the essential growth bound of $\left(A + DG(\mathbf{w}^\star)\right)_{\overline{D(A)}}$ is strictly negative.*

Proof. First of all, let us show that A is a Hille-Yosida operator. Consider $\lambda \in \mathbb{C}$ such that $\Re(\lambda) > 0$ and $(a, \psi) \in X$, then

$$(\lambda \mathbb{I} - A)^{-1} \begin{pmatrix} a \\ \psi \end{pmatrix} = \begin{pmatrix} 0 \\ \phi \end{pmatrix} \Leftrightarrow \begin{cases} \phi(0) = a \\ \phi' + \lambda\phi = \psi \end{cases}$$
$$\Leftrightarrow \phi(y) = ae^{-\lambda y} + \int_0^y \psi(s) e^{-\lambda(y-s)}\mathrm{d}s, \ y \in [0, +\infty).$$

Using definition (A.4), we can compute directly

$$\begin{aligned} \left\|(\lambda \mathbb{I} - A)^{-1} \begin{pmatrix} a \\ \psi \end{pmatrix}\right\|_X &= \left\| \begin{pmatrix} 0 \\ \phi \end{pmatrix} \right\|_X = |0| + \frac{1}{\omega(0)} \int_0^\infty \|\phi\|_{L^1((0,+\infty),\omega(x)\mathrm{d}x)} \\ &\leq \frac{1}{\omega(0)} \int_0^\infty |a| e^{-\lambda y} \omega(y)\mathrm{d}y \\ &+ \frac{1}{\omega(0)} \int_0^\infty \omega(y) \int_0^y |\psi(s)| e^{-\lambda(y-s)}\mathrm{d}s\mathrm{d}y, \\ &\leq \frac{|a|}{F(\lambda, 0)} \int_0^\infty F(\lambda, y)\mathrm{d}y \\ &+ \frac{1}{\omega(0)} \int_0^\infty |\psi(s)|\omega(s) \frac{1}{F(\lambda, s)} \int_s^\infty F(\lambda, y)\mathrm{d}y\mathrm{d}s, \end{aligned}$$

with $F(\lambda, x) := \omega(x)e^{-\lambda x}$.
We now introduce the following technical result.

Lemma 5. *Let $\omega : [0, +\infty) \to \mathbb{R}^+$. We define for $\lambda \in \mathbb{C}$ and $x \geq 0$, $F(\lambda, x) := \omega(x)e^{-\lambda x}$. If for some $\lambda_1 > 0$, the function $x \mapsto F(\lambda_1, x)$ is decreasing on $[0, +\infty)$, then for all $\lambda > \lambda_1$ and all $s \geq 0$, we have*

$$\frac{1}{F(\lambda, s)} \int_s^\infty F(\lambda, y)\mathrm{d}y \leq \frac{1}{\lambda - \lambda_1}.$$

Proof of Lemma 5. We first observe that $\dfrac{F(\lambda, y)}{F(\lambda_1, y)} = e^{-(\lambda-\lambda_1)y}$. By assumption, $F(\lambda_1, \cdot)$ is decreasing, so for all $y \geq s \geq 0$, $\dfrac{F(\lambda_1, y)}{F(\lambda_1, s)} \leq 1$. Hence, for all $\lambda > \lambda_1$ and $s \geq 0$,

$$\begin{aligned}\frac{1}{F(\lambda, s)} \int_s^\infty F(\lambda, y)\mathrm{d}y &= \frac{F(\lambda_1, s)}{F(\lambda, s)} \int_s^\infty \frac{F(\lambda_1, y)}{F(\lambda_1, s)} \frac{F(\lambda, y)}{F(\lambda_1, y)}\mathrm{d}y \\ &\leq e^{(\lambda-\lambda_1)s} \int_s^\infty e^{-(\lambda-\lambda_1)y}\mathrm{d}y = \frac{1}{\lambda - \lambda_1}.\end{aligned}$$

□

To apply Lemma 5, we now verify that $x \mapsto F(\lambda_1, x)$ is decreasing for some $\lambda_1 > 0$. We compute $\partial_x F_1(\lambda_1, x) = \big(\omega'(x) - \lambda_1\omega(x)\big)e^{-\lambda_1 x}$. Therefore, $\partial_x F_1(\lambda_1, x) \leq 0$ if and only if $\lambda_1 \geq \frac{\omega'(x)}{\omega(x)}$ for all $x \geq 0$. Using the definition of ω in (A.3) and of χ in (A.1), we compute

$$\frac{\omega'}{\omega} = \left(g' + g\frac{l'}{1+l}\right) \circ \chi^{-1}.$$

By assumptions (H2) and (H3), g' and $g\frac{l'}{1+l}$ are bounded, so there exists λ_1 such that $\lambda_1 \geq \sup_{x\geq 0} \frac{\omega'(x)}{\omega(x)}$. This guarantees that $F(\lambda_1, \cdot)$ is decreasing and hence Lemma 5 applies. Therefore,

$$\left\|(\lambda\mathbb{I} - A)^{-1}\begin{pmatrix} a \\ \psi \end{pmatrix}\right\|_X \leq \frac{1}{\lambda - \lambda_1}\left(|a| + \frac{1}{\omega(0)}\int_0^\infty |\psi(s)|\omega(s)ds\right) \leq \frac{\left\|\begin{pmatrix} a \\ \psi \end{pmatrix}\right\|_X}{\lambda - \lambda_1}.$$

So for all $\lambda > \lambda_1$,

$$\left\|(\lambda\mathbb{I} - A)^{-1}\right\|_{\mathcal{L}(X)} \leq \frac{1}{\lambda - \lambda_1},$$

and for all $n \geq 1$,

$$\|(\lambda\mathbb{I} - A)^{-n}\|_{\mathcal{L}(X)} \leq \left\|(\lambda\mathbb{I} - A)^{-1}\right\|^n_{\mathcal{L}(X)} \leq \frac{1}{(\lambda - \lambda_1)^n}.$$

Hence, A is a Hille-Yosida operator.
We now turn to the second part of the proposition, which concerns the essential growth bound of the linearized operator. From Eq. (A.7), we can write $DG(\mathbf{w}^\star)$ as the sum of two linear operators as follows

$$DG(\mathbf{w}^\star)\begin{pmatrix} 0 \\ \phi \end{pmatrix} = B\begin{pmatrix} 0 \\ \phi \end{pmatrix} + C\begin{pmatrix} 0 \\ \phi \end{pmatrix}$$

where $B : \overline{D(A)} \to X$ is the bounded linear operator defined by

$$B\begin{pmatrix} 0 \\ \phi \end{pmatrix} = \begin{pmatrix} 0 \\ -(\frac{\sigma}{f(L^\star)} + m)\phi \end{pmatrix}, \tag{A.8}$$

and $C : \overline{D(A)} \to X$ is defined by

$$C\begin{pmatrix} 0 \\ \phi \end{pmatrix} = P(\phi)\begin{pmatrix} \frac{\rho}{g(r_{\min})}\frac{f'(L^\star)}{f(L^\star)^2} \\ -\sigma\frac{f'(L^\star)}{f(L^\star)^2}w^\star \end{pmatrix}, \tag{A.9}$$

where the linear map $P : \mathrm{L}^1((0, +\infty), \omega(x)\mathrm{d}x) \to \mathbb{R}$ is given by

$$P(\psi) = \int_0^\infty k(x)\psi(x)\mathrm{d}x, \quad \forall \psi \in \mathrm{L}^1((0, +\infty), \omega(x)\mathrm{d}x). \tag{A.10}$$

By the Riesz-Fréchet-Kolmogorov theorem, we can check that P defined by Eq. (A.10) is a compact bounded linear operator. As A is a Hille-Yosida operator, B is bounded linear and C is compact bounded linear, we can apply Theorem 1.2. in Ducrot et al. (2008) to state that the essential growth bound of $(A + DG(\mathbf{w}^\star))_{\overline{D(A)}} = (A + B + C)_{\overline{D(A)}}$ is less than or equal to the essential growth bound of $(A + B)_{\overline{D(A)}}$. Furthermore, by corollary IV.2.10 in Engel and Nagel (2000), the essential growth bound of $(A + B)_{\overline{D(A)}}$ is less than or equal to the growth bound of $(A + B)_{\overline{D(A)}}$. Then, to state the negativity of the essential growth bound of $(A + DG(\mathbf{w}^\star))_{\overline{D(A)}}$, it is enough to show that the growth bound of $(A + B)_{\overline{D(A)}}$ is negative. Using the characteristic method, we show that $(A + B)_{\overline{D(A)}}$ generates a C^0-semigroup $\{T_{(A+B)_{\overline{D(A)}}}(t)\}_{t\geq 0}$ on $\overline{D(A)}$ defined by

$$T_{(A+B)_{\overline{D(A)}}}(t)\begin{pmatrix} 0 \\ \phi \end{pmatrix} = \begin{pmatrix} 0 \\ \hat{T}_{(A+B)_{\overline{D(A)}}}(t)(\phi) \end{pmatrix},$$

where

$$\hat{T}_{(A+B)_{\overline{D(A)}}}(t)(\phi)(x) = \begin{cases} \phi(x-t)e^{-\int_{x-t}^x (m(y) + \frac{\sigma}{f(L^\star)})\mathrm{d}y} & \text{if } x \geq t, \\ 0 & \text{otherwise.} \end{cases}$$

To compute the norm of $T_{(A+B)_{\overline{D(A)}}}(t)$ thereafter, we need the following expression

$$\exp\left(-\int_\xi^x m(y)dy\right) = \exp\left(-\int_\xi^x g' \circ \chi^{-1}(y)dy\right) = \frac{g\circ\chi^{-1}(\xi)}{g\circ\chi^{-1}(x)}, \tag{A.11}$$

coming from the change of variable $z = \chi^{-1}(y)$ in the integral and the expression (A.1) of χ. Then,

$$\left\|T_{(A+B)_{\overline{D(A)}}}(t)\begin{pmatrix} 0 \\ \phi \end{pmatrix}\right\|_X = \frac{1}{\omega(0)}e^{-t\frac{\sigma}{f(L^\star)}}\int_t^\infty \omega(x)|\phi(x-t)|e^{-\int_{x-t}^x m(y)\mathrm{d}y}\mathrm{d}x$$

and by using expression (A.11) and using the definition (A.3) of ω we obtain that

$$\begin{aligned}\left\|T_{(A+B)_{\overline{D(A)}}}(t)\begin{pmatrix} 0 \\ \phi \end{pmatrix}\right\|_X &= \frac{1}{\omega(0)}e^{-t\frac{\sigma}{f(L^\star)}}\int_0^\infty \omega(x+t)\frac{g(\chi^{-1}(x))}{g(\chi^{-1}(x+t))}|\phi(x)|\mathrm{d}x \\ &= \frac{1}{\omega(0)}e^{-t\frac{\sigma}{f(L^\star)}}\int_0^\infty \big(g(\chi^{-1}(x)) + l(\chi^{-1}(x+t))g(\chi^{-1}(x))\big)|\phi(x)|\mathrm{d}x.\end{aligned}$$

Let us now find an estimate for the integrand, considering separately $[0, x_1]$ and $[x_1, +\infty)$, where x_1 will be precised later on. In what follows, we denote by c all the constants (that do not depend on x or t) that may change from line to line.
One can note that from the definition of χ and the mean value inequality we have that $\chi^{-1}(x + t) - \chi^{-1}(x) \leq t\bar{g}$ where $\bar{g} := \max_{x\geq 0} g(x)$ and, as l is increasing, that

$$l(\chi^{-1}(x + t)) \leq l(\chi^{-1}(x) + t\bar{g}).$$

First, for $x \in [0, x_1]$, from assumptions (H2)-(H4), for all $\lambda > 0$,

$$\begin{aligned}g(\chi^{-1}(x)) + l(\chi^{-1}(x + t))g(\chi^{-1}(x)) &\leq c + cl(\chi^{-1}(x) + t\bar{g}) \\ &\leq c + ce^{\lambda(\chi^{-1}(x)+t\bar{g})} \leq ce^{\lambda\bar{g}t}.\end{aligned}$$

We choose λ such that $0 < \lambda < \frac{\sigma}{2f(L^\star)\bar{g}}$ and, as $\omega(x) \geq \min\omega > 0$ on $[0, x_1]$, we have

$$g(\chi^{-1}(x)) + l(\chi^{-1}(x + t))g(\chi^{-1}(x)) \leq c\frac{\omega(x)}{\omega(x)}e^{\frac{\sigma}{2f(L^\star)}t} \leq c\omega(x)e^{\frac{\sigma}{2f(L^\star)}t}.$$

Now, we define $x_1 = \chi(x_0)$, where x_0 is given at assumption (H3). Then, for $x \geq x_1$ and $t > \frac{x_0}{\bar{g}}$, with (H3) and (H2)-(H4),

$$l(\chi^{-1}(x + t)) \leq l(\chi^{-1}(x) + t\bar{g}) \leq cl(\chi^{-1}(x))l(t\bar{g}) \leq cl(\chi^{-1}(x))e^{t\frac{\sigma}{2f(L^\star)}}.$$

So, we have the same bound as before, using expression (A.3) for ω,

$$g(\chi^{-1}(x)) + l(\chi^{-1}(x + t))g(\chi^{-1}(x)) \leq c\omega(x)e^{\frac{\sigma}{2f(L^\star)}t}.$$

Hence,

$$\begin{aligned}&e^{-t\frac{\sigma}{f(L^\star)}}\frac{1}{\omega(0)}\int_0^\infty \big(g(\chi^{-1}(x)) + l(\chi^{-1}(x + t))g(\chi^{-1}(x))\big)|\phi(x)|\mathrm{d}x \\ &\leq ce^{-t\frac{\sigma}{2f(L^\star)}}\frac{1}{\omega(0)}\int_0^\infty \omega(x)|\phi(x)|\mathrm{d}x.\end{aligned}$$

So, finally, for t large enough, namely $t > \frac{x_0}{\bar{g}}$, we have the following bound

$$\left\| T_{(A+B)_{\overline{D(A)}}}(t)\begin{pmatrix}0\\ \phi\end{pmatrix}\right\|_X \leq ce^{-t\frac{\sigma}{2f(L^\star)}}\left\|\begin{pmatrix}0\\ \phi\end{pmatrix}\right\|_X.$$

Therefore the growth bound of $(A+B)_{\overline{D(A)}}$ is negative, and, as a consequence, the essential growth bound of $(A+DG(\mathbf{w}^\star))_{\overline{D(A)}}$ is negative too. □

As the maximum between the spectral bound of $\left(A+DG(\mathbf{w}^\star)\right)_{\overline{D(A)}}$ and its essential growth bound is equal to the maximum of the growth bound of its associated semigroup (corollary IV.2.11 in Engel and Nagel (2000)), we can study the asymptotic of the linearized problem by studying the spectral bound of $\left(A+DG(\mathbf{w}^\star)\right)_{\overline{D(A)}}$ or equivalently the spectral bound of $A+DG(\mathbf{w}^\star)$, see Lemma 2.2.10 in Magal and Ruan (2018). This is the aim of Proposition 6.

Proposition 6.

$$\sigma(A+DG(\mathbf{w}^\star))\cap\left\{\lambda\in\mathbb{C}:\Re(\lambda)>-\frac{\sigma}{f(L^\star)}\right\}$$
$$=\left\{\lambda\in\mathbb{C}:\Re(\lambda)>-\frac{\sigma}{f(L^\star)}\ \textit{and}\ \Delta(\lambda)=0\right\}$$

with

$$\Delta(\lambda)=1-\frac{\rho f'(L^\star)}{f^2(L^\star)}\int_0^\infty l\circ\chi^{-1}(x)\exp\left(-\left(\frac{\sigma}{f(L^\star)}+\lambda\right)x\right)\mathrm{d}x$$
$$+\frac{\rho\sigma f'(L^\star)}{f^3(L^\star)}\int_0^\infty l\circ\chi^{-1}(x)\exp\left(-\frac{\sigma}{f(L^\star)}x\right)\frac{1}{\lambda}\left(1-e^{-\lambda x}\right)\mathrm{d}x.$$

Proof. First, for the sake of readability, for all λ such that $\Re(\lambda)>-\frac{\sigma}{f(L^\star)}$, we define the function $\Theta\in\mathrm{L}^1((0,+\infty),\omega(x)\mathrm{d}x)$ as follows

$$\Theta(x)=e^{-\int_0^x(\lambda+m(\xi)+\frac{\sigma}{f(L^\star)})\mathrm{d}\xi},\quad\forall x\in[0,+\infty),$$

and the linear map $\mathcal{L}:\mathrm{L}^1((0,+\infty),\omega(x)\mathrm{d}x)\to\mathrm{L}^1((0,+\infty),\omega(x)\mathrm{d}x)$

$$\mathcal{L}(\psi)(x)=\int_0^x\psi(\xi)e^{-\int_\xi^x(\lambda+m(\eta)+\frac{\sigma}{f(L^\star)})\mathrm{d}\eta}\mathrm{d}\xi,$$
$$\forall\psi\in\mathrm{L}^1((0,+\infty),\omega(x)\mathrm{d}x),\forall x\in[0,+\infty).$$

We obtain from the definitions of A in (A.5) and B in (A.8)

$$(\lambda I-(A+B))\begin{pmatrix}0\\ \phi\end{pmatrix}=\begin{pmatrix}\phi(0)\\ \phi'+\left(\lambda+m(\cdot)+\frac{\sigma}{f(L^\star)}\right)\phi\end{pmatrix}.$$

Hence, by a calculation similar to the one in the proof of Proposition 4, the resolvent operator of $A+B$ is, for $\lambda\in\mathbb{C}$, $\Re(\lambda)>-\frac{\sigma}{f(L^\star)}$,

$$(\lambda I-(A+B))^{-1}\begin{pmatrix}a\\ \psi\end{pmatrix}=\begin{pmatrix}0\\ a\Theta(x)+\mathcal{L}(\psi)\end{pmatrix}.$$

Moreover, one can check that if $(\lambda I-(A+B))$ is invertible, then $(\lambda I-(A+B+C))$ is invertible if and only if $I-C(\lambda I-(A+B))^{-1}$ is invertible, and we have

$$(\lambda I-(A+B+C))^{-1}=(\lambda I-(A+B))^{-1}\left[I-C(\lambda I-(A+B))^{-1}\right]^{-1}.$$

By (A.9), we have

$$I-C(\lambda I-(A+B))^{-1}\begin{pmatrix}a\\ \psi\end{pmatrix}=\begin{pmatrix}a\\ \psi\end{pmatrix}-P(a\Theta(x)+\mathcal{L}(\psi))\begin{pmatrix}c_1\\ -c_2w^*\end{pmatrix},$$

with P defined in Eq. (A.10), $c_1=\frac{\rho}{g(r_{\min})}\frac{f'(L^\star)}{f(L^\star)^2}$ and $c_2=\sigma\frac{f'(L^\star)}{f(L^\star)^2}$. Then,

$$I-C(\lambda I-(A+B))^{-1}\begin{pmatrix}a\\ \psi\end{pmatrix}=\begin{pmatrix}\hat{a}\\ \hat{\psi}\end{pmatrix}$$
$$\Leftrightarrow\begin{cases}\hat{a}=a-c_1P(a\Theta+\mathcal{L}(\psi)),\\ \hat{\psi}=\psi+c_2P(a\Theta+\mathcal{L}(\psi))w^\star.\end{cases}\tag{A.12}$$

By applying $P\circ\mathcal{L}$ to the second equation and by linearity, we obtain

$$\begin{cases}\hat{a}=a\left(1-c_1P(\Theta)\right)-c_1P(\mathcal{L}(\psi)),\\ P(\mathcal{L}(\hat{\psi}))=P(\mathcal{L}(\psi))\left(1+c_2P(\mathcal{L}(w^\star))\right)+ac_2P(\Theta)P(\mathcal{L}(w^\star)).\end{cases}$$

Therefore a and $P(\mathcal{L}(\psi))$ are solutions of a linear system, i.e.

$$\begin{pmatrix}1-c_1P(\Theta) & -c_1\\ c_2P(\Theta)P(\mathcal{L}(w^\star)) & 1+c_2P(\mathcal{L}(w^\star))\end{pmatrix}\begin{pmatrix}a\\ P(\mathcal{L}(\psi))\end{pmatrix}=\begin{pmatrix}\hat{a}\\ P(\mathcal{L}(\hat{\psi}))\end{pmatrix}.$$

The determinant of the matrix is given by

$$\Delta(\lambda):=(1-c_1P(\Theta))(1+c_2P(\mathcal{L}(w^\star)))+c_1c_2P(\Theta)P(\mathcal{L}(w^\star))\tag{A.13}$$
$$=1-c_1P(\Theta)+c_2P(\mathcal{L}(w^\star)).$$

Therefore, if $\Delta(\lambda)\neq0$, then $I-C(\lambda I-(A+B))^{-1}$ is invertible, so, as explained before, $(\lambda I-(A+B+C))$ is invertible too, which implies that

$$\left\{\lambda\in\mathbb{C}:\Re(\lambda)>-\frac{\sigma}{f(L^\star)}\ \text{and}\ \Delta(\lambda)\neq0\right\}$$
$$\subset\rho(\lambda I-(A+B+C))\cap\left\{\lambda\in\mathbb{C}:\Re(\lambda)>-\frac{\sigma}{f(L^\star)}\right\},$$

or equivalently

$$\sigma(\lambda I-(A+B+C))\cap\left\{\lambda\in\mathbb{C}:\Re(\lambda)>-\frac{\sigma}{f(L^\star)}\right\}$$
$$\subset\left\{\lambda\in\mathbb{C}:\Re(\lambda)>-\frac{\sigma}{f(L^\star)}\ \text{and}\ \Delta(\lambda)=0\right\}.$$

On the other hand, let us show that if $\Delta(\lambda)=0$, we can find $\begin{pmatrix}a\\ \psi\end{pmatrix}\in X\setminus\{0\}$ such that $I-C(\lambda I-(A+B))^{-1}\begin{pmatrix}a\\ \psi\end{pmatrix}=0$, which is equivalent to find $\begin{pmatrix}0\\ \phi\end{pmatrix}\in D(A)\setminus\{0\}$ in the kernel of $\lambda I-(A+B+C)$. We set $a\neq0$ and $\psi:=-ac_2P(\Theta)w^\star+\frac{ac_2^2}{c_1}P(\mathcal{L}(w^\star))w^\star$. Then, as $\Delta(\lambda)=0$,

$$P(\mathcal{L}(\psi))=-ac_2P(\Theta)P(\mathcal{L}(w^\star))+\frac{ac_2^2}{c_1}P(\mathcal{L}(w^\star))^2$$
$$=\frac{ac_2}{c_1}P(\mathcal{L}(w^\star))(\Delta(\lambda)-1)=-\frac{ac_2}{c_1}P(\mathcal{L}(w^\star)),$$

so

$$\psi+c_2P(a\Theta+\mathcal{L}(\psi))w^\star=\frac{ac_2^2}{c_1}P(\mathcal{L}(w^\star))w^\star+c_2P(\mathcal{L}(\psi))w^\star$$
$$=\frac{ac_2^2}{c_1}P(\mathcal{L}(w^\star))w^\star-\frac{ac_2^2}{c_1}P(\mathcal{L}(w^\star))w^\star=0.$$

Furthermore,

$$a-c_1P(a\Theta+\mathcal{L}(\psi))=a-ac_1P(\Theta)+ac_2P(\mathcal{L}(w^\star))=a\Delta(\lambda)=0.$$

Hence, from (A.12), $I-C(\lambda I-(A+B))^{-1}\begin{pmatrix}a\\ \psi\end{pmatrix}=0$, thus

$$\left\{\lambda\in\mathbb{C}:\Re(\lambda)>-\frac{\sigma}{f(L^\star)}\ \text{and}\ \Delta(\lambda)=0\right\}$$
$$\subset\sigma(\lambda I-(A+B+C))\cap\left\{\lambda\in\mathbb{C}:\Re(\lambda)>-\frac{\sigma}{f(L^\star)}\right\}.$$

Finally, we simplify the expression of Δ given by (A.13). First, by replacing all the notations, substituting the expression of $w^\star=u^\star\circ\chi^{-1}$ from formula (8) and using formula (A.11), the expression (A.13) becomes equivalent to

$$\Delta(\lambda)=1-\frac{\rho}{g(r_{\min})}\frac{f'(L^\star)}{f^2(L^\star)}\int_0^\infty l(\chi^{-1}(x))g(\chi^{-1}(x))e^{-\int_0^x\frac{\sigma}{f(L^\star)}+\lambda+g'(\chi^{-1}(\eta))\mathrm{d}\eta}\mathrm{d}x$$
$$+\frac{\sigma\rho f'(L^\star)}{f^3(L^\star)}\int_{r_{\min}}^\infty l(\chi^{-1}(x))g(\chi^{-1}(x))e^{-\frac{\sigma}{f(L^\star)}x}\int_0^x\frac{1}{g(\chi^{-1}(\xi))}e^{-\int_\xi^x(\lambda+g'(\chi^{-1}(\eta)))\mathrm{d}\eta}\mathrm{d}\xi\mathrm{d}x,$$

where we recall that $\chi(x) := \int_{r_{\min}}^{x} \frac{1}{g(s)} \mathrm{d}s$. Hence, with the change of variables $r = \chi^{-1}(x)$ in both integral terms and $y = \chi^{-1}(\xi)$ in the integral within the second integral term, we obtain

$$\Delta(\lambda) = 1 - \frac{f'(L^\star)}{f^2(L^\star)} \int_{r_{\min}}^{\infty} q(r) \exp\left(-\left(\frac{\sigma}{f(L^\star)} + \lambda\right)\chi(r)\right)\mathrm{d}r$$
$$+ \frac{\sigma f'(L^\star)}{f^3(L^\star)} \int_{r_{\min}}^{\infty} q(r) \exp\left(-\frac{\sigma}{f(L^\star)}\chi(r)\right)\left(\int_{r_{\min}}^{r} \frac{1}{g(y)} \exp\left(-\lambda \int_{y}^{r} \frac{1}{g(z)}\mathrm{d}z\right)\mathrm{d}y\right)\mathrm{d}r,$$

where $q(r) := \rho \frac{l(r)}{g(r)}$. With a change of variables $\eta(y) = \chi(r) - \chi(y)$ in the integral within the second integral term, we can verify that

$$\Delta(\lambda) = 1 - \frac{f'(L^\star)}{f^2(L^\star)} \int_{r_{\min}}^{\infty} q(x) \exp\left(-\left(\frac{\sigma}{f(L^\star)} + \lambda\right)\chi(x)\right)\mathrm{d}x$$
$$+ \frac{\sigma f'(L^\star)}{f^3(L^\star)} \int_{r_{\min}}^{\infty} q(x) \exp\left(-\frac{\sigma}{f(L^\star)}\chi(x)\right)\left(\int_{0}^{\chi(x)} e^{-\lambda\eta}\mathrm{d}\eta\right)\mathrm{d}x.$$

Finally, with the change of variable $z = \chi(x)$, recalling that p is defined in (17) by $p = l \circ \chi^{-1}$, we obtain

$$\Delta(\lambda) = 1 - \frac{\rho f'(L^\star)}{f^2(L^\star)} \int_{0}^{\infty} p(z) \exp\left(-\left(\frac{\sigma}{f(L^\star)} + \lambda\right)z\right)\mathrm{d}z$$
$$+ \frac{\rho\sigma f'(L^\star)}{f^3(L^\star)} \int_{0}^{\infty} p(z) \exp\left(-\frac{\sigma}{f(L^\star)}z\right)\left(\int_{0}^{z} e^{-\lambda y}\mathrm{d}y\right)\mathrm{d}z$$
$$= 1 - \frac{\rho f'(L^\star)}{f^2(L^\star)} \int_{0}^{\infty} p(z) \exp\left(-\left(\frac{\sigma}{f(L^\star)} + \lambda\right)z\right)\mathrm{d}z$$
$$+ \frac{\rho\sigma f'(L^\star)}{f^3(L^\star)} \int_{0}^{\infty} p(z) \exp\left(-\frac{\sigma}{f(L^\star)}z\right)\frac{1}{\lambda}\left(1 - e^{-\lambda z}\right)\mathrm{d}z.$$

□

Appendix B. Figures

On Sup. Fig. B.6, we show the evolution of solution to system (1)–(2)–(4) with respect to time. The numerical simulation presented here is performed in two steps. First, a numerical resolution of PDE (1) is computed with a standard Euler explicit scheme in time and upwind finite volume scheme in space. Second, the extracellular lipid amount is updated with the new density thanks to Eq. (4). The upwind finite volume scheme is particularly easy to implement here since the velocity is always positive.

We start from an initial cell size distribution, where all the cells are empty and therefore the whole quantity of lipids $L_0 = 10$ nmol is outside cells. At early times, the lipids enter cells progressively, until nearly no extracellular lipids are left (Sup. Fig. B.6, top left panel). More precisely, at early times, radii are increasing and radius of 11μm is reached at $t = 100$, 13μm at $t = 200$, 15μm at $t = 300$ and 17μm at $t = 300$, see on bottom left panel of Sup. Fig. B.6. Then, at around $t = 900$, a peak of adipocytes with a very small radius appears and those cells are growing until the stationary distribution is reached (Sup. Fig. B.6, bottom right panel). We notice that the extracellular quantity of lipids is oscillating before reaching the stationary value, see on top right panel of Sup. Fig. B.6. This is coherent with the analytical result of the article since the eigenvalues of the linearized system are complex with a strictly negative real part, which leads to an oscillating behavior of the system.

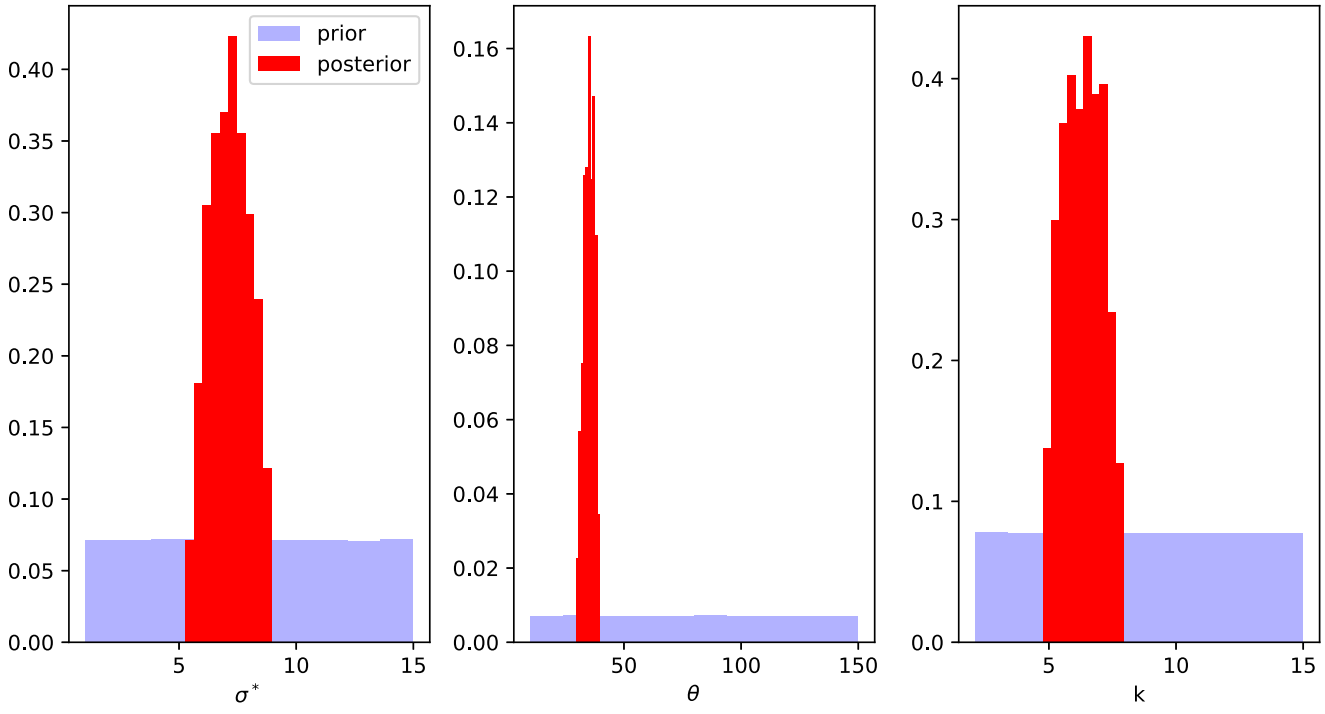

Fig. B.5. Prior and posterior parameter distributions from ABC rejection sampler algorithm. The posterior parameter distributions are obtained with cell size distribution of rat 1. The procedure was repeated 10^6 times and the threshold was set to $5\,10^{-4}$.

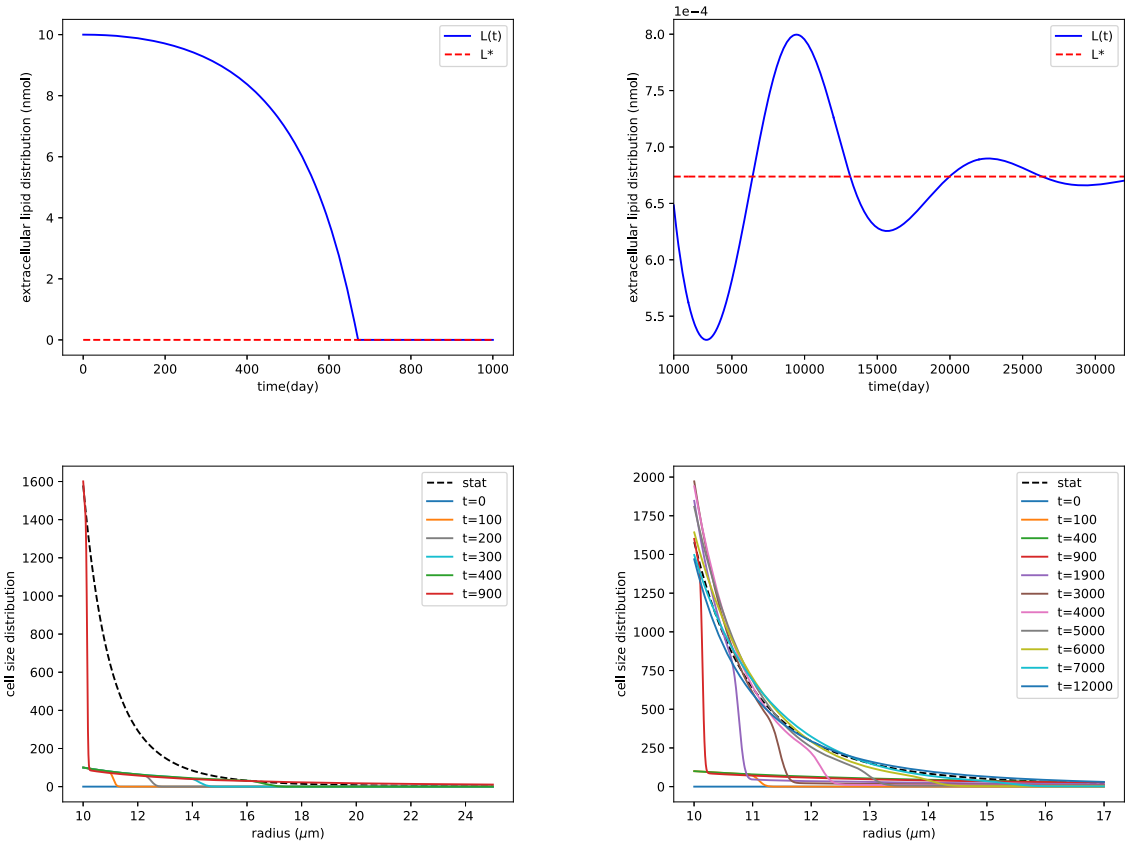

Fig. B.6. Time evolution of solutions of system (1)–(2)–(4). Top left: evolution of the extracellular lipid quantity with respect to time for early times ($0 \leq t \leq 1000$). Top right: evolution of the extracellular lipid quantity with respect to time for large times ($1000 \leq t \leq 32,000$). Bottom left: cell size distribution with respect to radius for different early times ($0 \leq t \leq 900$). Only the left part of the distribution is displayed (radius between 10 μm and 25 μm). Bottom right: cell size distribution with respect to radius for several times ($0 \leq t \leq 12,000$). Only the left part of the distribution is displayed (radius between 10μm and 17μm). Parameters are: $k = 6$, $\theta = 50\mu$m, $\alpha = 10^{-4}\mu\text{m}^{-1}.\text{time}^{-1}$, $\sigma = 5.10^{-4}$ time^{-1}, $r_{\min} = 10\mu$m.

References

Bernard, S., 2013. How to build a multiscale model in biology. Acta Biotheor. 61, 291–303. https://doi.org/10.1007/s10441-013-9199-z

Cabeza De Baca, T., Parrington, S., Votruba, S., Piaggi, P., Krakoff, J., Chang, D.C., 2024. Adipocyte size, adipose tissue calories, and circulating adipokines, before and after diet-induced weight loss in humans. Endocrine 84 (2), 490–499. https://doi.org/10.1007/s12020-023-03666-3

Calvo, J., Hingant, E., Yvinec, R., 2021. The initial-boundary value problem for the Lifshitz–Slyozov equation with non-smooth rates at the boundary. Nonlinearity 34 (4), 1975–2017. https://doi.org/10.1088/1361-6544/abd3f3

Cinti, S., Mitchell, G., Barbatelli, G., Murano, I., Ceresi, E., Faloia, E., Wang, S., Fortier, M., Greenberg, A.S., Obin, M.S., 2005. Adipocyte death defines macrophage localization and function in adipose tissue of obese mice and humans. J. Lipid Res. 46 (11), 2347–2355. https://doi.org/10.1194/jlr.M500294-JLR200

Clément, F., Fostier, L., Yvinec, R., 2024. Well-posedness and bifurcation analysis of a size-structured population model: Application to female gametes dynamics. https://hal.science/hal-04699357.

Collet, J.-F., Goudon, T., 2000. On solutions of the Lifshitz–Slyozov model. Nonlinearity 13 (4), 1239. https://doi.org/10.1088/0951-7715/13/4/314

Dauger, A., Soula, H., Audebert, C., 2025. Adipocyte size distribution: mathematical model of a tissue property. Math. Biosci. 384, 109433. https://doi.org/10.1016/j.mbs.2025.109433

Divoux, A., Clément, K., 2011. Architecture and the extracellular matrix: the still unappreciated components of the adipose tissue. Obes. Rev. 12, 494–503. https://doi.org/10.1111/j.1467-789X.2010.00811.x

Ducrot, A., Liu, Z., Magal, P., 2008. Essential growth rate for bounded linear perturbation of non-densely defined cauchy problems. J. Math. Anal. Appl. 341 (1), 501–518.

Engel, K.-J., Nagel, R., 2000. One-Parameter Semigroups for Linear Evolution Equations. Springer-Verlag, New York.

Ghaben, A.L., Scherer, P.E., 2019. Adipogenesis and metabolic health. Nat. Rev. Mol. Cell Biol. 20, 242–258. https://doi.org/10.1038/s41580-018-0093-z

Giacobbi, A.-S., Meyer, L., Ribot, M., Yvinec, R., Soula, H., Audebert, C., 2024. Mathematical modeling of adipocyte size distributions: identifiability and parameter estimation from rat data. J. Theor. Biol. 581, 111747. https://doi.org/10.1016/j.jtbi.2024.111747

Gliemann, J., Vinten, J., 1974. Lipogenesis and insulin sensitivity of single fat cells. J. Physiol. 236 (3), 499–516. https://doi.org/10.1113/jphysiol.1974.sp010449

Grabosch, A., Heijmans, H.J.A.M., 1990. Cauchy problems with state-dependent time evolution. Japan J. Appl. Math. 7 (3), 433–457. https://doi.org/10.1007/BF03167853

Grabosch, A., Heijmans, H. J.A.M., 1991. Production, development, and maturation of red blood cells. In: Arino, O., Axelrod, D.E., Kimmel, M. (Eds.), Mathematical Population Dynamics. CRC Press, pp. 189–210. https://doi.org/10.1201/9781003072706-15

Han, S.M., Nahmgoong, H., Yim, K.M., Kim, J.B., 2025. How obesity affects adipocyte turnover. Trend. Endocrinol. Metabol. 36 (2), 147–160. https://doi.org/10.1016/j.tem.2024.07.004

Hansen, F.M., Nielsen, J.H., Gliemann, J., 1974. The influence of body weight and cell size on lipogenesis and lipolysis of isolated rat fat cells*. Eur. J. Clin. Invest. 4 (1), 411–418. https://doi.org/10.1111/j.1365-2362.1974.tb00414.x

Jacquier, M., Crauste, F., Soulage, C.O., Soula, H.A., 2014. A predictive model of the dynamics of body weight and food intake in rats submitted to caloric restrictions. PLoS ONE 9(6), e100073. https://doi.org/10.1371/journal.pone.0100073

Jo, J., Gavrilova, O., Pack, S., Jou, W., Mullen, S., Sumner, A.E., Cushman, S.W., Periwal, V., 2009. Hypertrophy and/or hyperplasia: dynamics of adipose tissue growth. PLoS Comput. Biol. 5 (3), e1000324. https://doi.org/10.1371/journal.pcbi.1000324

Jo, J., Guo, J., Liu, T., Mullen, S., Hall, K.D., Cushman, S.W., Periwal, V., 2010. Hypertrophy-driven adipocyte death overwhelms recruitment under prolonged weight gain. Biophys J. 99 (11), 3535–3544. https://doi.org/10.1016/j.bpj.2010.10.009

Jo, J., Shreif, Z., Periwal, V., 2012. Quantitative dynamics of adipose cells. Adipocyte 1, 80–88. https://doi.org/10.4161/adip.19705

Kim, S.M., Lun, M., Wang, M., Senyo, S.E., Guillermier, C., Patwari, P., Steinhauser, M.L., 2014. Loss of white adipose hyperplastic potential is associated with enhanced susceptibility to insulin resistance. Cell Metab. 20 (6), 1049–1058.

Lafontan, M., Berlan, M., 1995. Fat cell $\alpha 2$ -adrenoceptors: the regulation of fat cell function and lipolysis*. Endocr. Rev. 16 (6), 716–738. https://doi.org/10.1210/edrv-16-6-716

Laurençot, P., 2001. Weak solutions to the lifshitz-slyozov-wagner equation. Indiana Univ. Math. J. 50 (3), 1319–1346.

Le Lay, S., Krief, S., Farnier, C., Lefrère, I., Le Liepvre, X., Bazin, R., Ferré, P., Dugail, I., 2001. Cholesterol, a cell size-dependent signal that regulates glucose metabolism and gene expression in adipocytes. J. Biol. Chem. 276 (20), 16904–16910. https://doi.org/10.1074/jbc.M010955200

Lim, Y., Boster, J., 2025. Obesity and Comorbid Conditions. StatPearls Publishing, Treasure Island (FL). http://www.ncbi.nlm.nih.gov/books/NBK574535/.

Liu, A., Sonmez, A., Yee, G., Bazuine, M., Arroyo, M., Sherman, A., McLaughlin, T., Reaven, G., Cushman, S., Tsao, P., 2010. Differential adipogenic and inflammatory properties of small adipocytes in zucker obese and lean rats. Diabet. Vascul. Dis. Res. 7 (4), 311–318. https://doi.org/10.1177/1479164110386126

MacKellar, J., Cushman, S.W., Periwal, V., 2010. Waves of adipose tissue growth in the genetically obese zucker fatty rat. PLoS ONE 5. https://doi.org/10.1371/journal.pone.0008197

Magal, P., Ruan, S., 2018. Theory and applications of abstract semilinear Cauchy problems. Vol. 201 of *Appl. Math. Sci.* Springer International Publishing.

McLaughlin, T., Sherman, A., Tsao, P., Gonzalez, O., Yee, G., Lamendola, C., Reaven, G.M., Cushman, S.W., 2007. Enhanced proportion of small adipose cells in insulin-resistant vs insulin-sensitive obese individuals implicates impaired adipogenesis. Diabetologia 50 (8), 1707–1715. https://doi.org/10.1007/s00125-007-0708-y

Meyer, L., Ribot, M., Yvinec, R., 2024. A lifshitz–slyozov type model for adipocyte size dynamics: limit from becker–döring system and numerical simulation. J. Math. Biol. 88 (2), 16. https://doi.org/10.1007/s00285-023-02036-x

Neese, R.A., Misell, L.M., Turner, S., Chu, A., Kim, J., Cesar, D., Hoh, R., Antelo, F., Strawford, A., McCune, J.M., Christiansen, M., Hellerstein, M.K., 2002. Measurement in vivo of proliferation rates of slow turnover cells by 2h2o labeling of the deoxyribose moiety of DNA. Proc. Natl. Acad. Sci. 99 (24), 15345–15350. https://doi.org/10.1073/pnas.232551499

Rigamonti, A., Brennand, K., Lau, F., Cowan, C.A., 2011. Rapid cellular turnover in adipose tissue. PLoS ONE 6 (3), e17637.

Sakers, A., De Siqueira, M.K., Seale, P., Villanueva, C.J., 2022. Adipose-tissue plasticity in health and disease. Cell 185, 419–446. https://doi.org/10.1016/j.cell.2021.12.016

Santoro, N., Kursawe, R., D'Adamo, E., Dykas, D.J., Zhang, C.K., Bale, A.E., Calí, A.M., Narayan, D., Shaw, M.M., Pierpont, B., Savoye, M., Lartaud, D., Eldrich, S., Cushman, S.W., Zhao, H., Shulman, G.I., Caprio, S., 2010. A common variant in the patatin-like phospholipase 3 gene (PNPLA3) is associated with fatty liver disease in obese children and adolescents. Hepatology 52 (4), 1281–1290. https://doi.org/10.1002/hep.23832

Sethi, J.K., Vidal-Puig, A.J., 2007. Thematic review series: adipocyte biology. adipose tissue function and plasticity orchestrate nutritional adaptation. J. Lipid Res. 48, 1253–1262. https://doi.org/10.1194/jlr.R700005-JLR200

Skurk, T., Alberti-Huber, C., Herder, C., Hauner, H., 2007. Relationship between adipocyte size and adipokine expression and secretion. J. Clin. Endocrinol. Metabol. 92 (3), 1023–1033. https://doi.org/10.1210/jc.2006-1055

Smith, U., 1971. Effect of cell size on lipid synthesis by human adipose tissue in vitro. J. Lipid Res. 12 (1), 65–70. https://doi.org/10.1016/S0022-2275(20)39547-X

Soula, H.A., Géloën, A., Soulage, C.O., 2015. Model of adipose tissue cellularity dynamics during food restriction. J. Theor. Biol. 364, 189–196. https://doi.org/10.1016/j.jtbi.2014.08.046

Soula, H.A., Julienne, H., Soulage, C.O., Géloën, A., 2013. Modelling adipocytes size distribution. J. Theor. Biol. 332, 89–95. https://doi.org/10.1016/j.jtbi.2013.04.025

Spalding, K.L., Arner, E., Westermark, P.O., Bernard, S., Buchholz, B.A., Bergmann, O., Blomqvist, L., Hoffstedt, J., Näslund, E., Britton, T., Concha, H., Hassan, M., Rydén, M., Frisén, J., Arner, P., 2008. Dynamics of fat cell turnover in humans. Nature 453 (7196), 783–787. https://doi.org/10.1038/nature06902

Toni, T., Welch, D., Strelkowa, N., Ipsen, A., Stumpf, M. P.H., 2009. Approximate bayesian computation scheme for parameter inference and model selection in dynamical systems. J. R. Soc. Interf. 6, 187–202. https://doi.org/10.1098/rsif.2008.0172

Trayhurn, P., 2013. Hypoxia and adipose tissue function and dysfunction in obesity. Physiol. Rev. 93 (1), 1–21. https://doi.org/10.1152/physrev.00017.2012

Turner, L., Gauthier, M.-F., Lafortune, A., Tchernof, A., Santosa, S., 2022. Adipocyte size, adipose tissue fibrosis, macrophage infiltration and disease risk are different in younger and older individuals with childhood versus adulthood onset obesity. Int. J. Obes. 46 (10), 1859–1866. https://doi.org/10.1038/s41366-022-01192-2

Wan, Y. C.E., Dufau, J., Spalding, K.L., 2024. Local and systemic impact of adipocyte senescence-associated secretory profile. Curr. Opin. Endocrine Metabol. Res. 37, 100547. https://doi.org/10.1016/j.coemr.2024.100547